Excess IL-18 drives fatal mousepox cytokine storm via NK cell immunodeficiency and nonspecific T-cell hyperactivation

Jemy A. Varghese[1,4]

Leonardo Huang[1]

Stephen D. Carro[2]

Emily Landy[3]

Anastasia Frank-Kamenetskii[1]

Hannah Klinghoffer[1]

Jeremy Morrissette[1,4]

Vinh Dang[1]

Laurence C. Eisenlohr[2,4]

Scott W. Canna[1,4]

[1]Rheumatology and Immune Dysregulation, Children's Hospital of Philadelphia, Philadelphia, Pennsylvania, United States

[2]Department of Pathology and Laboratory Medicine, Children's Hospital of Philadelphia, Philadelphia, Pennsylvania, United States

[3]Department of Immunology, University of Pittsburgh, Pittsburgh, Pennsylvania, United States

[4]Institute for Immunology and Immune Health, Perelman School of Medicine, University of Pennsylvania, Philadelphia, Pennsylvania, United States

Abstract:

Hemophagocytic Lymphohistiocytosis (HLH) is a hyperinflammatory syndrome with multiple contributors, often including an infectious trigger. The Macrophage Activation Syndrome (MAS) subtype is linked to marked IL-18 excess, cytotoxic T-lymphocyte (CTL) activation, and natural killer (NK) cell abnormalities. We asked how excess IL-18 shapes NK and CTL responses to viral challenge. Mice with chronic IL-18 overproduction (*Il18*^{tg}), showed baseline NK-cytopenia and CTL activation resembling MAS-susceptible patients. NK transcriptomes reflected IL-18/IFNg-axis activation and cell cycle upregulation. LCMV infection of *Il18*^{tg} mice causes HLH/MAS without affecting viral control, but is not a significant NK challenge. Early after infection with NK-dependent mousepox, *Il18*^{tg} NKs failed to activate appropriately, but CTLs quickly hyperactivated and mousepox control remained intact. Mousepox-infected *Il18*^{tg} mice then developed signs of HLH/MAS including hepatosplenic necrosis. Their viral control was impaired, possibly because they failed to expand mousepox-specific CTLs. *Il18bp*^{KO} mice, despite more normal resting lymphocytes, succumbed similarly to viremic HLH/MAS. Transfer of pre-activated NKs into *Il18*^{tg} mice partially rescued virus-specific CTL responses, viral control, and survival. Thus, excess IL-18 contributes to HLH/MAS via disparate effects on CTL and NK cells, demonstrating a novel, context-specific NK immunodeficiency and highlighting how subtle host-pathogen interactions can affect the mechanisms and treatment rationale of life-threatening HLH/MAS.

Introduction:

Hemophagocytic Lymphohistiocytosis (HLH) is a complex, multifactorial syndrome of systemic inflammation, coagulopathy, cytopenias, hepatitis, and hyperferritinemia. Mechanistically, HLH is canonically associated with biallelic defects that cripple granule-mediated cytotoxicity (GMC), as seen in Familial HLH (FHL). FHL is exceedingly rare; the great majority of patients meeting clinical HLH criteria have intact GMC and secondary HLH (sHLH) arising from infectious, malignant, cancer immunotherapy, and/or rheumatic causes(1). The latter, better known as Macrophage Activation Syndrome (MAS), is largely described in Still's Disease and Systemic Juvenile Idiopathic Arthritis, where it is strongly linked to the cytokine IL-18(2).

Infection-associated HLH (IA-HLH) can occur in patients with intact immune systems and nearly any pathogen can serve as a trigger. Primary EBV infection is by far the best-described, followed by other DNA viruses and (largely intracellular) microbes(1). The distinction between IA-HLH and severe sepsis is unclear(3). Infection is a common HLH trigger in other forms of HLH. Children with FHL are typically healthy at birth, developing signs of HLH in the first few months of life presumably initiated by infection. EBV is also a classic trigger for primary HLH in genetically-susceptible individuals (e.g. *SH2D1A*, *XIAP*, *CD27*, ...)(4-7). In MAS, at least 34% of episodes involve an infectious trigger, and again EBV is reported most commonly(8).

Seeking causal overlap between MAS and FHL, heterozygous "carrier" variants in FHL-associated GMC genes appear to be enriched in MAS patients(9-11). However, more recent work has emphasized a unique role for IL-18 in MAS. IL-18 is an inflammasome-activated cytokine best known for acting on NK cells, activated/memory T Cells, and Chimeric Antigen

Receptor (CAR) T Cells to induce Interferon-g (IFNg) and promote GMC(2, 12). Profoundly elevated levels of IL-18 often exceed neutralization by IL-18 binding protein (IL-18BP) and serve as a uniquely specific diagnostic biomarker of MAS-prone disorders, so-called "IL-18opathies"(2, 13-16). The discovery of several monogenic autoinflammatory IL-18opathies(2, 17-21), and a small but growing experience with IL-18 blockade(22-24), help place excess IL-18 upstream of MAS.

Animal models of HLH/MAS have been essential to our understanding of this complex immunobiology. The arenavirus Lymphocytic Choriomeningitis Virus (LCMV) is a common mouse pathogen cleared readily in wild-type (WT) mice. As in human perforin deficiency (FHL2)(25), *Prf1*^{KO} mice appear normal at rest, but LCMV infection leads to persistent viremia and drives murine HLH via unopposed antigen presentation, CD8+ cytotoxic T-lymphocyte (CTL) hyperactivation, and IFNg overproduction(26, 27). Similarly, IL-18 transgenic mice (*Il18*^{tg}) constitutively overexpress mature IL-18 (driven by hEμ enhancer/mIgVH promotor) and develop normally(28). Upon LCMV infection, their CTL become hyperactivated and overproduce IFNg, leading to HLH/MAS(29-31). Unlike *Prf1*^{KO} mice, however, *Il18*^{tg} mice clear LCMV normally and their T-cell contraction and memory formation are ultimately normal(29). In mice and in vitro, IL-18 synergizes with GMC impairment and preferentially promotes CTL activation(2, 29-31).

The role of NK cells in HLH and MAS remains unclear. NK cytotoxic function is impaired in FHL but also non-specifically in acutely ill patients; it is no longer part of the HLH clinical criteria(32). In mice, perforin-expressing NK cells temper inflammation in models of FHL2(33) and SJIA(34). MAS patients show NK cytopenia and impaired NK cell function(35-

39). Given these observations, and NK cells' responsiveness to IL-18, we sought to evaluate the effects of excess IL-18 on NK cell number and function in vivo.

Results

At rest, Il18^{tg} mice show NK and CTL changes reminiscent of Still's disease

Given the association of high serum IL-18 and NK cytopenia/dysfunction in Still's Disease and MAS(35, 38, 40, 41), we profiled NK cells and NK-like type 1 Innate Lymphoid Cells (ILC1) in mice with transgenic expression of mature IL-18 (*Il18^{tg}*)(28). Resting *Il18^{tg}* mice demonstrated fewer NK cells, particularly in livers, spleens, and bone marrow (Figure 1A), whereas ILC1 were similar to WT (Supplemental Figure 1A). *Il18^{tg}* NKs also showed decreased expression of maturity markers CD11b and CD49b relative to WT (Figure 1B, Supplemental Figure 1B). Consistent with Still's patients' NK cell IL-18 insensitivity(35, 38), NK cell IL-18 receptor expression was also significantly decreased in *Il18^{tg}* mice (Figure 1B).

Transcriptome analysis of spleen and liver NK cells isolated directly ex vivo showed slightly greater expression of candidate "type 1" immune activation genes (e.g *Prf1*, *GzmB*, *Ifng, Klrc3, Cd226, Csf1*) and lower *Il18r1* expression in *Il18^{tg}* mice (Supplemental Figure 2A, Supplemental Data 1). Tissue-adjusted Differential Gene Expression (DGE) analysis demonstrated modest upregulation of interferon stimulated genes (ISGs). Gene Set Enrichment Analysis (GSEA) of the murine "Immunologic Signature" (MSigDB M7) gene sets showed consistent enrichment of gene sets associated with systemic IL-18/IFNg exposure in *Il18^{tg}* vs. WT NK cells, driven by genes induced by or participating in IFN signaling (e.g. *B2m, CD274, Stat1/2, Tap1, Usp18, Zbp1*). Similarly, we observed modest enrichment for genes upregulated by ex vivo IL-18 stimulation of NK cells (Supplemental Data 2). Analysis of the "Canonical

Pathway" (MSigDB M2) gene sets identified cell cycle and antigen presentation pathway enrichment (Supplemental Figure 2B, Supplemental Data 1).

Finding normal total NK cell number in peripheral blood, but fewer in tissues, we hypothesized that NK cells in *Il18*^{tg} mice might be short-lived in the periphery. In bone marrow and spleen, we observed a lower proportion of NK cells expressing markers of maturity (CD27^{-} CD11b^{+}) and greater proportion expressing markers of NK immaturity (CD11b^{-}CD27^{+}) (42) in *Il18*^{tg} mice (Figure 1C-D). We saw enrichment of an "immature NK" gene set (generated from existing data(43)) in *Il18*^{tg} vs WT tissue NK cells, but this was driven by genes like *Dpp4* (CD26), *Cd3d/g*, and *Ikzf2* (Helios) (see Supplemental Methods, Supplemental Data 3). We could not assess *Il18*^{tg} NK cell function ex vivo due to their dismal survival (Figure 1E). Together, their decreased numbers, IL-18/IFNg axis activation pattern, and poor ex vivo survival suggest that even at rest, NK cells from *Il18*^{tg} mice are poised for activation-induced cell death. This is consistent with reports that in vitro IL-18 stimulation promotes human NK cell death(30, 44). By contrast, and consistent with our prior observations(30), *Il18*^{tg} mice showed a modest expansion of highly activated (CD44^{+}PD1^{+}), predominantly CD8^{+} T cells across all organs surveyed (Figure 2, Supplemental Figure 3).

Infection with the mousepox (ectromelia) virus intensifies Il18^{tg} *NK cell deficiency and CTL hyperactivation*.

We previously found that infection of *Il18*^{tg} mice with LCMV (Armstrong strain) induced HLH via CTL hyperactivation without compromising viral clearance(29-31). LCMV is a non-lytic, single-stranded RNA arenavirus and NK cells contribute little to its handling or clearance in mice(26, 45). By contrast, the lytic DNA mousepox/Ectromelia virus (ECTV, Moscow strain)

is a significant in vivo challenge to NK function. Like LCMV, WT mice typically survive mousepox and clear virus a few weeks after infection. Unlike LCMV, depletion or impairment of NK cells in WT mice subverts early viral control, resulting in diminished T-cell responses, and fatal organ dysfunction; but NK-depleted mice lack the overwhelming T-cell activation characteristic of HLH(46, 47)(48)·(49).

Five days after ECTV infection, both WT and *Il18*^{tg} hepatic NK cells had expanded, although *Il18*^{tg} NK numbers remained lower than WT. Likewise, infection induced the expected increases in activation/maturation markers CD49b and IL-18Rα in WT mice, but failed to appreciably promote NK activation in *Il18*^{tg} mice (Figures 3A-B, Supplemental Figure 4). Despite their lackluster NK response, *Il18*^{tg} mice controlled ECTV at the early timepoints associated with NK cell function, and serum IFNg levels were comparable between WT and *Il18*^{tg} mice (Figures 3C-D, Supplemental Figure 5). *Il18*^{tg} CTL, already activated prior to infection,

expanded and became further activated at early timepoints after ECTV infection (Figures 3A, E). Given the contrast between their diminished NK cell responses and normal cytokine production/viral load, we predicted that NK/ILC1 depletion of *Il18*^{tg} mice would have minimal effect on their ECTV load. Depleting NK1.1-expressing cells prior to and during infection, we observed significantly increased ECTV RNA in WT mice, but a much smaller effect in *Il18*^{tg} (Figure 3F). NK depletion did not diminish the robust CTL activation in *Il18*^{tg} mice, and modestly affected systemic IFNg levels in WT (Figure 3G-H).

Il18^{tg} *mice ultimately develop fulminant HLH/MAS following ECTV infection.*

As expected, WT mice demonstrated modest weight loss beginning 6-7 days post infection. *Il18*^{tg} mice behaved similarly at first, but then quickly deteriorated with weight loss, anemia, thrombocytopenia, hepatic and splenic infarcts, profound hepatitis, and ultimately a high degree of morbidity (Figures 4A-E). The immune response in WT mice began with NK expansion at day 4 that was soon dwarfed by the expansion of activated CTL. *Il18*^{tg} mice, by contrast, experienced a far less impressive NK expansion whereas activated CTL cell numbers rose by day 2 and plateaued until day 8 (Figures 4F-G). Myeloid cells, predominantly monocytes/macrophages, expanded consistently throughout (Figures 4H). Despite being able to clear LCMV infection(29-31) and control ECTV normally through day 5, *Il18*^{tg} mice soon demonstrated failure to appropriately control virus in both spleens and livers (Figure 4I). Paralleling CTL hyperactivation, serum IFNg rose earlier and stayed elevated longer in *Il18*^{tg} mice (Figure 4J). Thus, infected *Il18*^{tg} mice showed both disordered CTL activation indicative of HLH/MAS and weak NK responses/impaired viral clearance indicative of immunodeficiency.

Despite normal-appearing NK cells at rest, Il18bp^{KO} *mice also develop severe viremic HLH/MAS following mousepox infection*.

To test the hypothesis that NK immunodeficiency in *Il18*^{tg} mice arose from chronic exposure to excess IL-18, we evaluated *Il18bp*^{KO} mice. IL-18 Binding Protein (IL-18BP) is a soluble antagonist, abundant at rest and IFNg-inducible, that binds to mature IL-18 with high affinity and prevents its signaling(16, 50). At rest, *Il18bp*^{KO} mice have normal blood IFNg levels(51), and we observed little effect on NK cell number or CD11b, CD49b, or IL-18R expression (Figure 5A, Supplemental Figure 1B). Despite this more normal start, splenic NK cells from *Il18bp*^{KO} mice also failed to expand or upregulate CD49b appropriately after ECTV

infection (Figure 5B). In contrast to *Il18*^{tg} mice, *Il18bp*^{KO} mice showed a significant impairment of ECTV control at Day 5 post-infection (Figure 5C).

At later timepoints, *Il18bp*^{KO} mice exhibited similar weight loss, cytopenias, IFNg elevation, hepatitis, and prolonged viremia as *Il18*^{tg} mice (Figure 5D-I). Notably, *Il18bp*^{KO} mice showed no significant differences in CD8 or CD4 T-cell activation relative to WT, although CD44^{+}PD-1^{+} CTL trended toward greater expansion in infected *Il18bp*^{KO} mice by later timepoints (Figure 5H, Supplemental Figure 3). Despite less profound CTL activation, *Il18bp*^{KO} mice showed elevated blood IFNg levels and collapsed hepatic architecture, with swaths of necrosis and early fibrosis (Figure 5F-G, Supplemental Figure 6).

To determine whether IL-18BP could be preventing this deadly response to mousepox infection by means other than restraining IL-18, we challenged mice with knock-out of both *Il18* and *Il18bp*. *Il18*^{KO}*;Il18bp*^{KO} mice resisted HLH/MAS, responding to mousepox infection similarly to WT mice (Supplemental Figure 7). Though *Il18*^{tg} mice appear transiently protected at very early timepoints, these data suggest that even acute excess of IL-18 can drive lethal responses to mousepox.

Excess IL-18 induces an ineffective virus-specific CTL response to mousepox infection.

We wondered why the rapid and robust CTL activation in ECTV-infected *Il18*^{tg} mice could not compensate for NK cell dysfunction and curtail fatality. To better understand pathogen-specific T-cell responses, we tracked ECTV-specific CD8 T Cells using tetramer staining for the immunodominant H-2K^{b}-B8R$^{20\text{-}27}$ epitope (B8R)(52). Whereas WT mice developed the anticipated, robust expansion of B8R-specific CTL, expansion of this population in *Il18*^{tg} livers and spleens was both delayed and significantly less pronounced (Figure 6A).

Similarly, in vivo killing assays(53) confirmed that infected *Il18*^{tg} mice were impaired in clearing B8R peptide-loaded target cells (Figure 6B), as well as target cells loaded with less immunodominant ECTV-peptides (Figure 6C). ECTV-tetramer+ CTL were more variably abundant in *Il18bp*^{KO} spleens, but these mice nevertheless showed impaired clearance of B8R-pulsed cells such that individual disease severity (as assessed by weight loss) directly correlated with the number of B8R-specific CTL (Figures 6D-F).

To better compare the timing and characteristics of activation marker upregulation and tetramer+ CTL expansion, we examined longitudinal patterns of splenic and hepatic CD8 T Cells over time in a single annotated Uniform Manifold Approximation and Projection (UMAP) (Figure 7A). WT mice did not show a substantial population of activated CTL (CD44^{+} or KLRG1^{+}) until around day 6. Quickly thereafter, nearly all CTL were activated, many specific for the B8R ECTV peptide, but few expressing inhibitory receptors like PD-1, Lag3, or TIGIT. By contrast, *Il18*^{tg} mice harbored substantial populations of activated CTL expressing inhibitory receptors as early as 2.5 days post-infection (Figure 7B-C). This included a small PD-1+CD44- population previously observed spontaneously in *Il18*^{tg}*;Prf1*^{KO} mice(30). Their activated CTL populations shifted inconsistently over time, but very few tetramer+ CTL ever developed. These data suggest that the failure to develop effective antigen-specific CTL in *Il18*^{tg} mice occurs despite robust but nonspecific CTL activation.

Activated NK cells protect Il18^{tg} *mice from ECTV-induced immunopathology*

Effective NK and virus-specific CTL responses are required sequentially for protection from mousepox(46, 54); and both *Il18*^{tg} and *Il18bp*^{KO} mice showed virus-specific CTL defects following mousepox but not LCMV infection(29). To determine whether WT NK cells could

231 rescue pathogen-specific responses and protect *Il18*^{tg} mice from fulminant mousepox infection,
232 we transferred ex vivo-expanded WT NK cells into *Il18*^{tg} mice one day prior to mousepox
233 infection (Figure 8A). Transfer of 5 million NK cells partially protected *Il18*^{tg} mice from
234 mortality, but not weight loss (of surviving mice, Figures 8B-C). Cultured NK cells showed
235 strong CD49b and IL-18R expression prior to transfer, mirroring WT NK cells early after ECTV
236 infection. However, recovery of transferred NK cells was minimal and only observed in recipient
237 livers. Recovered NKs were more uniformly C49b- and CD11b+ (Figures 8D-E). Nevertheless,
238 transfer of NK cells improved tetramer+ CTL responses and ECTV control in *Il18*^{tg} mice, albeit
239 not to levels observed in WT mice (Figures 8F-G). Weight loss and high serum IFNγ persisted
240 independently of viral control, suggesting these were direct hyperinflammatory effects of excess
241 IL-18 (Figure 8H).
242
243

Discussion:

HLH/MAS is a complex, life-threatening, systemic inflammatory state that overlaps conceptually and mechanistically with sepsis and Cytokine Release Syndrome. Though identifying patients "in HLH" is an important challenge(1), the most important task for clinicians managing HLH is targeting its contributors. This task is not simple. Many contributors are unknown, non-targetable, or difficult to identify (e.g. occult lymphoma); and they do not act in isolation. Additionally, individual contributors may act via multiple immunopathogenic mechanisms: *autoinflammation* involves excessive innate immune responses; *immunodeficiency* involves direct pathogen-induced damage due to defective pathogen control; and *hyperinflammation* is damage from excessive, pathogen-specific, adaptive immune responses.

IL-18 is likely more than a uniquely specific biomarker of MAS susceptibility(13, 14). We and others have shown that IL-18 drives HLH/MAS through *autoinflammatory* actions like IFNg amplification(13, 51), synergy with GMC impairment(29, 30), and promotion of inflammatory target cell death(31); and by *hyperinflammatory* actions like antigen-specific CTL hyperactivation(29). Herein, we describe a new, context-specific role for IL-18 as an inducer of NK *immunodeficiency*.

Even without MAS, Still's patients often have elevated free IL-18(14) capable of stimulating IL-18-responsive cells. Normal peripheral NK cell numbers in well-controlled Still's patients belie subtle NK abnormalities: transcriptionally, their NK cells have upregulated innate immune genes like *TLR4* and *S100A9*, and functionally they show specific defects with IL-18 responsiveness(35, 38, 39) (recapitulated in *Il18*^{tg} mice(29), Figure 1B). Active MAS patients' peripheral blood shows NK cytopenia and expansion of activated CD8 T Cells(38, 55, 56). NK cytopenia is common in most forms of secondary HLH(57) and even severe COVID-19(58), and

may correlate with a shared HLH/MAS immunophenotype of CTL and macrophage hyperactivation(55, 56, 59-61). Experimental evidence supports this shift from NK to CTL activation in MAS: both IL-18 and IL-6 appear to impair NK cell proliferation and survival(37, 44), and activated CD8 T Cells serve as a sink for IL-2, a key NK proliferation/survival signal(62). These trends are less clear in MAS/HLH tissues. Liver biopsies show abundant CD8 T lymphocytes and histiocytes, but most do not report NK cells(59, 63, 64). NK cells were present, but not pictured or quantified, in four predominantly lymphoma-associated HLH patients' liver biopsies(65). A review of FHL liver biopsies specifically noted the rarity of NK cells relative to CD8+ T Cells(66).

HLH/MAS also arises in most XIAP-deficients, typically triggered by EBV infection and associated with highly-elevated peripheral IL-18 levels. Though XIAP-deficiency may promote inflammasome activation in model systems, the mechanistic bases for its highly-elevated IL-18 and susceptibility to EBV are unknown(19, 67, 68). Excess IL-18 may also promote viremia and HLH/MAS in Kaposi's sarcoma herpesvirus (KSHV)-associated inflammatory disorders(69, 70). We found MAS-level IL-18 elevation in a small proportion of patients from infection-associated HLH(13) and hyperferritinemic sepsis(71) cohorts. Highly-elevated IL-18 levels may go undetected in other infection cohorts due to widespread hook effects in multiplex panels(13, 71).

Our observations in *Il18*^{tg} mice illustrate how NK defects may promote HLH/MAS. Like Still's patients, *Il18*^{tg} mice showed a basal state of mild NK cytopenia, CTL activation, and elevated IFNg, and NK cells struggled to survive ex vivo (Figure 1F). Transcriptome analysis validated IL-18/IFNg-axis upregulation. Cell cycle gene set enrichment, paired with surface expression of CD27 but not CD11b, supports proliferation and/or immaturity. NK cells in *Il18bp*^{KO} mice appeared more like WT under resting conditions, though more significant

290 *Il18bp*^{KO} NK defects have been observed in other facilities(72). Upon infection, IL-18 seemed to
291 impair expression of integrin-αM (CD11b) and -α2 (CD49b) more than activating receptors like
292 NKG2E and NKG2D(46, 73, 74). This suggests that IL-18 promoted an NK cell state of
293 susceptibility to activation-induced cell death (AICD); we observed similar effects on CTL(30).
294 These baseline defects engendered by IL-18, poising NK cells for AICD and amplifying global
295 CTL activation, were fatally exploited by mousepox.

296 Despite their inert NK cells, *Il18*^{tg} mice contained ECTV normally until day 5, possibly
297 due to basal IFNg produced by CD8 T Cells. *Il18bp*^{KO} mice, by contrast, quickly acquired the
298 problems present constitutively in *Il18*^{tg} mice. We speculate that the pre-existing pool of
299 activated CTL in *Il18*^{tg} (but not *Il18bp*^{KO}) mice served as a weak and temporary restraint on
300 ECTV at the earliest stages of infection. Both "excess IL-18 systems" then failed to mount
301 effective pathogen-specific CD8 T-cell responses. In this respect, IL-18 joins other NK defects
302 (e.g. loss of NKG2D, virulence factor inhibition of NK immune synapse formation, and aging-
303 related migration defects) in demonstrating that, specifically for complex lytic DNA viruses like
304 mousepox and murine cytomegalovirus (MCMV), robust NK responses are a requirement for
305 effective virus-specific CD8 T-cell responses(46, 47, 49, 75).

306 This study has several important limitations. Mousepox is an excellent in vivo NK
307 challenge, but not a human pathogen. Efforts to develop EBV-based models of HLH are
308 ongoing(76-78). Unlike XIAP deficiency, prolonged EBV viremia is not commonly reported in
309 MAS, although viremia in primary infection can last months and local reactivation is common
310 even in normal hosts(79). IL-18 mediated NK immunodeficiency may be local/transient and
311 serve to further boost IL-18's pathogenic effects. Additionally, the link between NK defects and
312 failed CTL responses requires elaboration. Robust but non-specific CD8 T-cell activation in

313 *Il18*^{tg} mice suggests NK cells are not required for CTL activation in general. Likewise, the
314 absence of a significant pool of pathogen-specific CTL at any timepoint argues against
315 exhaustion. Whether NK cells directly prime effective CTL responses to viruses like ECTV and
316 MCMV, or they simply keep viremia below an "organ failure threshold" beyond which mice
317 cannot support pathogen-specific CTL development, is not known. Other hypotheses, like NK
318 effects on antigen presentation, fractricide, and direct support of organ function, should be
319 explored. Notably, ECTV encodes a viral *IL18BP* homologue(80), perhaps enabling free IL-18
320 to function everywhere except near the infected cells where it is most needed.
321 Overall, this study shows how one cytokine may contribute to HLH via multiple
322 simultaneous mechanisms depending on the presence/nature of infectious trigger. IL-18's
323 auto/hyperinflammatory propensity for CD8 T-cell activation likely combines with its promotion
324 of NK AICD to drive MAS. Even in controlled murine models with specific triggers,
325 longitudinal quantitation of viral load, and detection of tetramer-labeled T Cells, we struggle to
326 apportion blame across IL-18's different immunopathologic mechanisms. In HLH patients,
327 attribution to one mechanism versus another might dramatically affect treatment strategy, but is
328 often practically impossible. The recent regulatory approval of IFNg blockade for steroid-
329 refractory MAS represents major progress(81), but not all MAS patients respond favorably. No
330 IL-18 blocking drugs are yet approved for clinical use, although multiple strategies are in
331 development and anecdotes have been encouraging(2). Neither acute IFNg nor IL-18 blockade
332 may be effective if the wheels of NK immunodeficiency and/or CTL hyperactivation are already
333 in motion. Our findings support assessment of IL-18 in HLH patients as part of a broad
334 assessment of likely contributors. However, they undermine the notion that HLH can be
335 successfully treated by targeting immune responses alone, underscoring individualized treatment

paradigms that balance immunomodulation with aggressive detection and clearance of contributing pathogens.

Materials and Methods

Sex as a biological variable: Our study examined male and female animals, and similar findings are reported for both sexes.

Mice, Infections, & NK Depletion: Adult mice aged 8-13 weeks were maintained, bred, and handled in specific pathogen free conditions under animal protocols approved by The University of Pittsburgh or The Children's Hospital of Philadelphia. Male and female mice were distributed equally across groups and analyzed together. Wild-type (WT) and *Il18*^{KO} mice were obtained from Jackson Laboratories. *Il18*^{tg} mice were generated by Tomoaki Hoshino (Kurume University, Kurume City)(28). *Il18bp*^{KO} mice (Il18bp$^{tm1.1(KOMP)Vlcg}$) were obtained from the knockout mouse project. Mice were genotyped by PCR using appropriate primers (**Supplemental Methods**). Mousepox ectromelia virus (ECTV, Moscow strain, 3000 pfu via hind footpad) infections were performed as in previous publications(29, 49). To deplete NK cells, mice were injected IP with 200ug of anti-NK1.1 (BioXCell, BE0036; clone PK136) or rat IgG2a isotype control (BioXCell, BE0090; clone LTF-2) -1 and +2 days after infection with ECTV.

Flow cytometry: Splenocytes were digested in media (DMEM+2%FBS) containing DNAse (100 µg/ml) and collagenase D (0.135U/ml) for 25-30 minutes, followed by mechanical disruption and osmotic (ACK) lysis. Livers were perfused in situ, collected into media, homogenized using gentleMACS tissue dissociator (Miltenyi), and digested in DNAse/collagenase as above. Bone marrow cells were isolated from tibias and/or femurs through hydrostatic extrusion using media, followed by mechanical disruption and RBC lysis. Whole blood was collected into pre-weighed EDTA tubes, plasma isolated by centrifugation, and

peripheral blood mononuclear cells (PBMC) isolated using Ficoll (GE Healthcare). Live cells were counted by Acridine Orange/Propidium Iodide on Nexcelom Cellometer K2.

Single cell suspensions were stained at 40C in HBSS for 30 minutes (see antibodies/reagents list in **Supplemental Methods)**. Cells were acquired on a 4-laser Beckman Coulter CytoFLEX S, 6-laser Beckman Coulter CytoFLEX LX, or five-laser Cytek Aurora system and analyzed using FlowJo™ version 10.10.0 (Treestar). All gating strategies are included in **Supplemental Methods**. UMAP was generated using FlowJo™ v11 integrated UMAP platform from the following parameters: B8R tetramer, CD44, TIGIT, Lag-3, CD11b, KLRG1, IL-18Rα, CD39, and PD-1; and with the following settings: number of nearest neighbors=15; minimum distance=0.5, distance metric=euclidean; number of components=2, total number of events=103,045 events gates as CD8 T cells.

In vivo killing assays: As in previous publications(29, 82), congenically-marked control and ECTV-peptide pulsed splenocytes were injected IV into mice 7-8 days post infection. ECTV-peptides included with B8R: H-2K^{b}-B8R$^{20-27}$, E7R: H-2K^{b}-E7R$^{130-137}$, J3R$^{289-296}$, or A3$^{270-277}$. Splenocyte groups were labeled with Tag-it Violet (Biolegend) or CellTrace™ CFSE, Yellow, or Far Red (Invitrogen) prior to transfer at equal ratios as assessed by flow cytometry of pre-injection mixture. Dye and peptide combinations were changed between replicates to minimize dye-specific variability. Transferred cells were recovered from recipient spleens 4 hours post-transfer and quantified by flow cytometry.

Virus Quantitation: Spleen and liver tissues were stored and digested in Trizol (Invitrogen) and RNA extracted with chloroform (Fisher Scientific) per manufacturer's instructions. First-strand cDNA was synthesized with qScript™ cDNA Synthesis Kits (Quantabio). For *18s* rRNA and *Evm003* qPCR was performed using Quantabio PerfeCTa® SYBR® Green SuperMix (see

Supplemental methods for primers) and quantitated on a QuantStudio™ 5 System. Normalized expression was calculated as $2^{(Cq^{Evm003} - Cq^{18s\ rRNA})}$. ECTV with replicative potential was assessed by plaque assay on BS-C-1 cells as in *Peauroi et al*(49) from organs also assessed by qPCR (**Supplemental Figure 5**).

Histology: Tissues were fixed in 10% buffered formalin (Fisher SF98-4) for 24 hours prior to processing, paraffin embedding, and sectioning (5um). Slides were stained with hematoxylin and eosin or Trichrome Stain LG Solution (Sigma Aldrich HT10316) and scored for liver damage by two independent, blinded reviewers using Leica DM4000B upright light microscope and Leica DFC7000 T camera. Liver damage was scored as in *Gasmi & Kleiner*(83) at 400x magnification as: involved area (0-25%=1; 25-50%=2; 50-75%=3; 75-100%=4) + degree of necrosis (0-2).

RNA-seq: Splenic NK, liver NK, and Liver ILC1 cells were purified by double-sorting, ~1,000 cells were sorted directly into lysis buffer, and library preparation was performed per manufacturer's instructions (Smart-Seq V4 ultra-low-input RNA sequencing preparation kit, Takara). Canonical NK cell transcripts were identified from MsigDB pathways (KEGG_NATURAL_KILLER_CELL_MEDIATED_CYTOTOXICITY, BIOCARTA_NKCELLS_PATHWAY) and Bezman et al.(84). See **Supplemental Methods** for details on Differential Gene Expression (DGE) analyses and generation of "NK IL-18 Response" and "Immature NK/ILC" custom gene sets.

Gene Set Enrichment Analysis (GSEA): After removing genes with group mean TPM<5, GSEA comparing *Il18*^{tg} vs WT for NK cells (combined liver and spleen) and ILC1 was performed using GSEAv4.2.3 and the following parameters: Gene sets=MSigDBM7 (Immunologic Signatures), M2 (Canonical Pathways), or custom gene sets as above; number of

permutations=1000; permutation type=gene_set. Heat maps were generated using Morpheus (Broad Institute).

NK culture and Expansion: Splenic NK cells were purified using MojoSort negative selection kit (Biolegend). To assess survival ex vivo, cells were cultured in complete medium (**Supplemental Methods**) for 5 hours and subsequently assessed for NK cell identity and viability by flow cytometry. For ex vivo activation/expansion, WT splenic NK cells were purified as above and cultured in complete medium supplemented with murine IL-2 (1000U/mL, PeproTech). Cells were split and media replaced every 3 days for 7-10 days, washed twice in PBS and injected IV on day -1 ($5x10^6$/mouse).

Statistical analyses: Frequentist statistical analyses were performed in GraphPad Prism v11.02 on data combined from multiple experiments as detailed in figure legends. For error bars, data represent mean ± SEM. Significance was defined as adjusted $p<0.05$.

Data Availability: Raw .fastq and partially-processed RNAseq data are available in the Gene Expression Omnibus: GSE307223. Values for all data points are reported in the **Supporting Data Values** file.

Manuscript Information

Author contributions: J.A.V and S.W.C. planned and performed experiments and wrote the manuscript. L.H., S.D.C., A.F-K., H.K., J.M. , and V.D. assisted in experiments and data collection; and J.A.V., S.W.C., E.L., and A.F.-K. analyzed data. L.C.E. and S.D.C. provided expertise and assisted intellectually.

AI disclosure: The authors declare that no AI tools were used in the original research for or writing of this article.

Conflict-of-interest statement: No authors have Ownership, Income, Research Support, or Intellectual Property conflicts of interest relevant to this work per JCI Insight guidelines. SC has served as consultant and clinical trial site PI (< $5000 per entity) for Novartis and AB2Bio related to IL-18 blocking drug development programs.

Funding support: This work was supported by R01HD098428 (PI S.W.C.), the RK Mellon Institute for Pediatric Research (UPMC Children's Hospital), and the CHOP Research Institute

Acknowledgments: The authors would like to acknowledge Giuseppe Sciume (Sapienza University, Rome) for assistance with in vitro NK cell RNAseq analysis; Elise Peauroi for helpful advice; Rania Elbakri, William MacDonald, and Amanda Poholek (University of Pittsburgh) for assistance with RNAseq library prep; Florin Tuluc and Jennifer Murray (CHOP Flow Cytometry Core Laboratory, RRID:SCR_009726) for assistance with Flow Cytometry experiments, the CHOP Research Institute Pathology Core for assistance with histology imaging, and the NIH Tetramer Core Facility for key reagents.

Address of correspondence: Scott W. Canna (cannas@chop.edu) 3615 Civic Center Blvd, Abramson Research Center 1110A, Philadelphia, PA 19104.

References

1. Shakoory B, Geerlinks A, Wilejto M, Kernan K, Hines M, Romano M, et al. The 2022 EULAR/ACR Points to Consider at the Early Stages of Diagnosis and Management of Suspected Haemophagocytic Lymphohistiocytosis/Macrophage Activation Syndrome (HLH/MAS). *Arthritis & rheumatology.* 2023;75(10):1714-32.
2. Landy E, Carol H, Ring A, and Canna S. Biological and clinical roles of IL-18 in inflammatory diseases. *Nat Rev Rheumatol.* 2024;20(1):33-47.
3. Canna SW, and Cron RQ. Highways to hell: Mechanism-based management of cytokine storm syndromes. *The Journal of allergy and clinical immunology.* 2020;146(5):949-59.
4. Canna SW, and Marsh RA. Pediatric hemophagocytic lymphohistiocytosis. *Blood.* 2020;135(16):1332-43.
5. Song Y, Wang Y, and Wang Z. Requirement for etoposide in the initial treatment of Epstein-Barr virus-associated haemophagocytic lymphohistiocytosis. *Br J Haematol.* 2019;186(5):717-23.
6. Shamriz O, Kumar D, Shim J, Briones M, Quarmyne MO, Chonat S, et al. T Cell-Epstein-Barr Virus-Associated Hemophagocytic Lymphohistiocytosis (HLH) Occurs in Non-Asians and Is Associated with a T Cell Activation State that Is Comparable to Primary HLH. *J Clin Immunol.* 2021;41(7):1582-96.
7. Liu M, Brodeur KE, Bledsoe JR, Harris CN, Joerger J, Weng R, et al. Features of hyperinflammation link the biology of Epstein-Barr virus infection and cytokine storm syndromes. *The Journal of allergy and clinical immunology.* 2024.
8. Minoia F, Davi S, Horne A, Demirkaya E, Bovis F, Li C, et al. Clinical features, treatment, and outcome of macrophage activation syndrome complicating systemic juvenile idiopathic arthritis: a multinational, multicenter study of 362 patients. *Arthritis & rheumatology.* 2014;66(11):3160-9.

9. Zhang K, Biroschak J, Glass DN, Thompson SD, Finkel T, Passo MH, et al. Macrophage activation syndrome in patients with systemic juvenile idiopathic arthritis is associated with MUNC13-4 polymorphisms. *Arthritis Rheum.* 2008;58(9):2892-6.

10. Kaufman KM, Linghu B, Szustakowski JD, Husami A, Yang F, Zhang K, et al. Whole-exome sequencing reveals overlap between macrophage activation syndrome in systemic juvenile idiopathic arthritis and familial hemophagocytic lymphohistiocytosis. *Arthritis & rheumatology.* 2014;66(12):3486-95.

11. Correia Marques M, Rubin D, Shuldiner EG, Datta M, Schmitz E, Gutierrez Cruz G, et al. Enrichment of Rare Variants of Hemophagocytic Lymphohistiocytosis Genes in Systemic Juvenile Idiopathic Arthritis. *Arthritis & rheumatology.* 2024;76(10):1566-72.

12. Svoboda J, Landsburg DJ, Gerson J, Nasta SD, Barta SK, Chong EA, et al. Enhanced CAR T-Cell Therapy for Lymphoma after Previous Failure. *The New England journal of medicine.* 2025;392(18):1824-35.

13. Weiss ES, Girard-Guyonvarc'h C, Holzinger D, de Jesus AA, Tariq Z, Picarsic J, et al. Interleukin-18 diagnostically distinguishes and pathogenically promotes human and murine macrophage activation syndrome. *Blood.* 2018;131(13):1442-55.

14. Krei JM, Møller HJ, and Larsen JB. The role of interleukin-18 in the diagnosis and monitoring of hemophagocytic lymphohistiocytosis/macrophage activation syndrome – a systematic review. *Clin Exp Immunol.* 2021;203(2):174-82.

15. Fautrel B, Mitrovic S, De Matteis A, Bindoli S, Anton J, Belot A, et al. EULAR/PReS recommendations for the diagnosis and management of Still's disease, comprising systemic juvenile idiopathic arthritis and adult-onset Still's disease. *Ann Rheum Dis.* 2024;83(12):1614-27.

16. Girard C, Rech J, Brown M, Allali D, Roux-Lombard P, Spertini F, et al. Elevated serum levels of free interleukin-18 in adult-onset Still's disease. *Rheumatology (Oxford).* 2016;55(12):2237-47.

17. Canna SW, de Jesus AA, Gouni S, Brooks SR, Marrero B, Liu Y, et al. An activating NLRC4 inflammasome mutation causes autoinflammation with recurrent macrophage activation syndrome. *Nat Genet.* 2014;46(10):1140-6.

18. Romberg N, Al Moussawi K, Nelson-Williams C, Stiegler AL, Loring E, Choi M, et al. Mutation of NLRC4 causes a syndrome of enterocolitis and autoinflammation. *Nat Genet.* 2014;46(10):1135-9.

19. Wada T, Kanegane H, Ohta K, Katoh F, Imamura T, Nakazawa Y, et al. Sustained elevation of serum interleukin-18 and its association with hemophagocytic lymphohistiocytosis in XIAP deficiency. *Cytokine.* 2014;65(1):74-8.

20. Gernez Y, de Jesus AA, Alsaleem H, Macaubas C, Roy A, Lovell D, et al. Severe autoinflammation in 4 patients with C-terminal variants in cell division control protein 42 homolog (CDC42) successfully treated with IL-1beta inhibition. *The Journal of allergy and clinical immunology.* 2019;144(4):1122-5 e6.

21. Lam MT, Coppola S, Krumbach OHF, Prencipe G, Insalaco A, Cifaldi C, et al. A novel disorder involving dyshematopoiesis, inflammation, and HLH due to aberrant CDC42 function. *J Exp Med.* 2019;216(12):2778-99.

22. Canna SW, Girard C, Malle L, de Jesus A, Romberg N, Kelsen J, et al. Life-threatening NLRC4-associated hyperinflammation successfully treated with IL-18 inhibition. *The Journal of allergy and clinical immunology.* 2017;139(5):1698-701.

23. Rood JE, Rezk A, Pogoriler J, Finn LS, Burnham JM, Josephson MB, et al. Improvement of Refractory Systemic Juvenile Idiopathic Arthritis-Associated Lung Disease with Single-Agent Blockade of IL-1beta and IL-18. *J Clin Immunol.* 2023;43(1):101-8.

24. Gabay C, Fautrel B, Rech J, Spertini F, Feist E, Kotter I, et al. Open-label, multicentre, dose-escalating phase II clinical trial on the safety and efficacy of tadekinig alfa (IL-18BP) in adult-onset Still's disease. *Ann Rheum Dis.* 2018;77(6):840-7.

25. Stepp SE, Dufourcq-Lagelouse R, Le Deist F, Bhawan S, Certain S, Mathew PA, et al. Perforin gene defects in familial hemophagocytic lymphohistiocytosis. *Science.* 1999;286(5446):1957-9.

26. Jordan MB, Hildeman D, Kappler J, and Marrack P. An animal model of hemophagocytic lymphohistiocytosis (HLH): CD8+ T cells and interferon gamma are essential for the disorder. *Blood.* 2004;104(3):735-43.

27. Jenkins MR, Rudd-Schmidt JA, Lopez JA, Ramsbottom KM, Mannering SI, Andrews DM, et al. Failed CTL/NK cell killing and cytokine hypersecretion are directly linked through prolonged synapse time. *J Exp Med.* 2015;212(3):307-17.

28. Hoshino T, Kawase Y, Okamoto M, Yokota K, Yoshino K, Yamamura K, et al. Cutting edge: IL-18-transgenic mice: in vivo evidence of a broad role for IL-18 in modulating immune function. *J Immunol.* 2001;166(12):7014-8.

29. Tsoukas P, Rapp E, Van Der Kraak L, Weiss ES, Dang V, Schneider C, et al. Interleukin-18 and cytotoxic impairment are independent and synergistic causes of murine virus-induced hyperinflammation. *Blood.* 2020;136(19):2162-74.

30. Landy E, Varghese J, Dang V, Szymczak-Workman A, Kane LP, and Canna SW. Complementary HLH susceptibility factors converge on CD8 T-cell hyperactivation. *Blood Adv.* 2023;7(22):6949-63.

31. Frank-Kamenetskii A, Klinghoffer H, Varghese J, Dang V, Morrissette J, Fraietta JA, et al. Modeling the HLH immune synapse uncovers critical roles for IS termination, cytokine intensity, and target cell death. *Blood.* 2025;146(5):558-70.

32. Henter JI, Sieni E, Eriksson J, Bergsten E, Hed Myrberg I, Canna SW, et al. Diagnostic guidelines for familial hemophagocytic lymphohistiocytosis revisited. *Blood.* 2024;144(22):2308-18.

33. Sepulveda FE, Maschalidi S, Vosshenrich CA, Garrigue A, Kurowska M, Menasche G, et al. A novel immunoregulatory role for NK-cell cytotoxicity in protection from HLH-like immunopathology in mice. *Blood.* 2015;125(9):1427-34.

34. Vandenhaute J, Avau A, Filtjens J, Malengier-Devlies B, Imbrechts M, Van den Berghe N, et al. Regulatory Role for NK Cells in a Mouse Model of Systemic Juvenile Idiopathic Arthritis. *J Immunol.* 2019;203(12):3339-48.

35. de Jager W, Vastert SJ, Beekman JM, Wulffraat NM, Kuis W, Coffer PJ, et al. Defective phosphorylation of interleukin-18 receptor beta causes impaired natural killer cell function in systemic-onset juvenile idiopathic arthritis. *Arthritis Rheum.* 2009;60(9):2782-93.

36. Avau A, Put K, Wouters CH, and Matthys P. Cytokine balance and cytokine-driven natural killer cell dysfunction in systemic juvenile idiopathic arthritis. *Cytokine & growth factor reviews.* 2015;26(1):35-45.

37. Cifaldi L, Prencipe G, Caiello I, Bracaglia C, Locatelli F, De Benedetti F, et al. Inhibition of natural killer cell cytotoxicity by interleukin-6: implications for the pathogenesis of macrophage activation syndrome. *Arthritis & rheumatology.* 2015;67(11):3037-46.

38. Put K, Vandenhaute J, Avau A, van Nieuwenhuijze A, Brisse E, Dierckx T, et al. Inflammatory Gene Expression Profile and Defective Interferon-gamma and Granzyme K in Natural Killer Cells From Systemic Juvenile Idiopathic Arthritis Patients. *Arthritis & rheumatology.* 2017;69(1):213-24.

39. Ohya T, Nishimura K, Murase A, Hattori S, Ohara A, Nozawa T, et al. Impaired Interleukin-18 Signaling in Natural Killer Cells From Patients With Systemic Juvenile Idiopathic Arthritis. *ACR Open Rheumatol.* 2022;4(6):503-10.

40. Grom AA, Villanueva J, Lee S, Goldmuntz EA, Passo MH, and Filipovich A. Natural killer cell dysfunction in patients with systemic-onset juvenile rheumatoid arthritis and macrophage activation syndrome. *J Pediatr.* 2003;142(3):292-6.

41. Villanueva J, Lee S, Giannini EH, Graham TB, Passo MH, Filipovich A, et al. Natural killer cell dysfunction is a distinguishing feature of systemic onset juvenile rheumatoid arthritis and macrophage activation syndrome. *Arthritis Res Ther.* 2005;7(1):R30-7.

42. Chiossone L, Chaix J, Fuseri N, Roth C, Vivier E, and Walzer T. Maturation of mouse NK cells is a 4-stage developmental program. *Blood.* 2009;113(22):5488-96.

43. Shih HY, Sciume G, Mikami Y, Guo L, Sun HW, Brooks SR, et al. Developmental Acquisition of Regulomes Underlies Innate Lymphoid Cell Functionality. *Cell.* 2016;165(5):1120-33.

44. Huang Y, Lei Y, Zhang H, Zhang M, and Dayton A. Role of interleukin-18 in human natural killer cell is associated with interleukin-2. *Molecular immunology.* 2010;47(16):2604-10.

45. Gallimore A, Glithero A, Godkin A, Tissot AC, Pluckthun A, Elliott T, et al. Induction and exhaustion of lymphocytic choriomeningitis virus-specific cytotoxic T lymphocytes visualized using soluble tetrameric major histocompatibility complex class I-peptide complexes. *J Exp Med.* 1998;187(9):1383-93.

46. Fang M, Lanier LL, and Sigal LJ. A role for NKG2D in NK cell-mediated resistance to poxvirus disease. *PLoS pathogens.* 2008;4(2):e30.

47. Fang M, Roscoe F, and Sigal LJ. Age-dependent susceptibility to a viral disease due to decreased natural killer cell numbers and trafficking. *J Exp Med.* 2010;207(11):2369-81.

48. Parker AK, Parker S, Yokoyama WM, Corbett JA, and Buller RM. Induction of natural killer cell responses by ectromelia virus controls infection. *J Virol.* 2007;81(8):4070-9.

583 49. Peauroi EM, Carro SD, Pei L, Reynoso GV, Hickman HD, and Eisenlohr LC. The ectromelia virus
584 virulence factor C15 facilitates early viral spread by inhibiting NK cell contact. *iScience.*
585 2022;25(12):105510.
586 50. Zhou T, Damsky W, Weizman OE, McGeary MK, Hartmann KP, Rosen CE, et al. IL-18BP is a
587 secreted immune checkpoint and barrier to IL-18 immunotherapy. *Nature.* 2020;583(7817):609-
588 14.
589 51. Girard-Guyonvarc'h C, Palomo J, Martin P, Rodriguez E, Troccaz S, Palmer G, et al. Unopposed IL-
590 18 signaling leads to severe TLR9-induced macrophage activation syndrome in mice. *Blood.*
591 2018;131(13):1430-41.
592 52. Remakus S, Rubio D, Ma X, Sette A, and Sigal LJ. Memory CD8+ T cells specific for a single
593 immunodominant or subdominant determinant induced by peptide-dendritic cell immunization
594 protect from an acute lethal viral disease. *J Virol.* 2012;86(18):9748-59.
595 53. Barber DL, Wherry EJ, and Ahmed R. Cutting edge: rapid in vivo killing by memory CD8 T cells. *J*
596 *Immunol.* 2003;171(1):27-31.
597 54. Rapaport AS, Schriewer J, Gilfillan S, Hembrador E, Crump R, Plougastel BF, et al. The Inhibitory
598 Receptor NKG2A Sustains Virus-Specific CD8(+) T Cells in Response to a Lethal Poxvirus Infection.
599 *Immunity.* 2015;43(6):1112-24.
600 55. De Matteis A, Colucci M, Rossi MN, Caiello I, Merli P, Tumino N, et al. Expansion of CD4dimCD8+
601 T cells characterizes macrophage activation syndrome and other secondary HLH. *Blood.*
602 2022;140(3):262-73.
603 56. Huang Z, Brodeur KE, Chen L, Du Y, Wobma H, Hsu EE, et al. Type I interferon signature and
604 cycling lymphocytes in macrophage activation syndrome. *J Clin Invest.* 2023;133(22).
605 57. Oh EJ, Yoon JH, Park KH, Bae HJ, Yun SJ, Min GJ, et al. Natural-killer cell cytotoxicity as a
606 diagnostic and prognostic marker for adult patients with secondary hemophagocytic

lymphohistiocytosis: a prospective phase II observational study. *Ther Adv Hematol.* 2021;12:20406207211020544.

58. Gallardo-Zapata J, and Maldonado-Bernal C. Natural killer cell exhaustion in SARS-CoV-2 infection. *Innate Immun.* 2022;28(6):189-98.

59. Billiau AD, Roskams T, Van Damme-Lombaerts R, Matthys P, and Wouters C. Macrophage activation syndrome: characteristic findings on liver biopsy illustrating the key role of activated, IFN-gamma-producing lymphocytes and IL-6- and TNF-alpha-producing macrophages. *Blood.* 2005;105(4):1648-51.

60. Segal JE, Daley JD, Barnum JL, Salgado CM, Reyes-Mugica M, Schneider C, et al. Systemic and Nodular Hyperinflammation in a Patient with Refractory Familial Hemophagocytic Lymphohistiocytosis 2. *J Clin Immunol.* 2021;41(5):987-91.

61. Chaturvedi V, Marsh RA, Zoref-Lorenz A, Owsley E, Chaturvedi V, Nguyen TC, et al. T-cell activation profiles distinguish hemophagocytic lymphohistiocytosis and early sepsis. *Blood.* 2021;137(17):2337-46.

62. Humblet-Baron S, Franckaert D, Dooley J, Bornschein S, Cauwe B, Schonefeldt S, et al. IL-2 consumption by highly activated CD8 T cells induces regulatory T-cell dysfunction in patients with hemophagocytic lymphohistiocytosis. *The Journal of allergy and clinical immunology.* 2016;138(1):200-9 e8.

63. Kim HA, Kwon JE, Yim H, Suh CH, Jung JY, and Han JH. The pathologic findings of skin, lymph node, liver, and bone marrow in patients with adult-onset still disease: a comprehensive analysis of 40 cases. *Medicine (Baltimore).* 2015;94(17):e787.

64. Eloseily E, Romankevych I, Sabit T, Berklite L, Ranganathan S, Rosen P, et al. Hepatic Manifestations in Systemic Juvenile Idiopathic Arthritis and Macrophage Activation Syndrome. *J Rheumatol.* 2026;53(6):669-78.

65. Bihl F, Emmenegger U, Reichen J, Neftel KA, Zimmermann A, and Cerny A. Macrophage activating syndrome is associated with lobular hepatitis and severe bile duct injury with cholestasis. *J Hepatol.* 2006;44(6):1208-12.

66. Chen JH, Fleming MD, Pinkus GS, Pinkus JL, Nichols KE, Mo JQ, et al. Pathology of the liver in familial hemophagocytic lymphohistiocytosis. *Am J Surg Pathol.* 2010;34(6):852-67.

67. Marsh RA, Madden L, Kitchen BJ, Mody R, McClimon B, Jordan MB, et al. XIAP deficiency: a unique primary immunodeficiency best classified as X-linked familial hemophagocytic lymphohistiocytosis and not as X-linked lymphoproliferative disease. *Blood.* 2010;116(7):1079-82.

68. Chiang SCC, Owsley E, Panchal N, Chaturvedi V, Terrell CE, Jordan MB, et al. Quercetin ameliorates XIAP deficiency-associated hyperinflammation. *Blood.* 2022;140(7):706-15.

69. Lage SL, Ramaswami R, Rocco JM, Rupert A, Davis DA, Lurain K, et al. Inflammasome activation in patients with Kaposi sarcoma herpesvirus-associated diseases. *Blood.* 2024;144(14):1496-507.

70. Rocco J, Manion M, Laidlaw E, Galindo F, Lage S, Rupert A, et al. *Cytokines 2023*. Athens, GR; 2023.

71. Carol HA, Mayer AS, Zhang MS, Dang V, Varghese J, Martinez Z, et al. Hyperferritinemia Screening to Aid Identification and Differentiation of Patients with Hyperinflammatory Disorders. *J Clin Immunol.* 2024;45(1):4.

72. Harms RZ, Creer AJ, Lorenzo-Arteaga KM, Ostlund KR, and Sarvetnick NE. Interleukin (IL)-18 Binding Protein Deficiency Disrupts Natural Killer Cell Maturation and Diminishes Circulating IL-18. *Frontiers in immunology.* 2017;8:1020.

73. Stotesbury C, Alves-Peixoto P, Montoya B, Ferez M, Nair S, Snyder CM, et al. alpha2beta1 Integrin Is Required for Optimal NK Cell Proliferation during Viral Infection but Not for

Acquisition of Effector Functions or NK Cell-Mediated Virus Control. *J Immunol.* 2020;204(6):1582-91.

74. Fang M, Orr MT, Spee P, Egebjerg T, Lanier LL, and Sigal LJ. CD94 is essential for NK cell-mediated resistance to a lethal viral disease. *Immunity.* 2011;34(4):579-89.

75. Waggoner SN, Cornberg M, Selin LK, and Welsh RM. Natural killer cells act as rheostats modulating antiviral T cells. *Nature.* 2011;481(7381):394-8.

76. Yin L, Al-Alem U, Liang J, Tong WM, Li C, Badiali M, et al. Mice deficient in the X-linked lymphoproliferative disease gene sap exhibit increased susceptibility to murine gammaherpesvirus-68 and hypo-gammaglobulinemia. *Journal of medical virology.* 2003;71(3):446-55.

77. Sato K, Misawa N, Nie C, Satou Y, Iwakiri D, Matsuoka M, et al. A novel animal model of Epstein-Barr virus-associated hemophagocytic lymphohistiocytosis in humanized mice. *Blood.* 2011;117(21):5663-73.

78. Wirtz T, Weber T, Kracker S, Sommermann T, Rajewsky K, and Yasuda T. Mouse model for acute Epstein-Barr virus infection. *Proc Natl Acad Sci U S A.* 2016;113(48):13821-6.

79. Balfour HH, Jr., Odumade OA, Schmeling DO, Mullan BD, Ed JA, Knight JA, et al. Behavioral, virologic, and immunologic factors associated with acquisition and severity of primary Epstein-Barr virus infection in university students. *J Infect Dis.* 2013;207(1):80-8.

80. Krumm B, Meng X, Li Y, Xiang Y, and Deng J. Structural basis for antagonism of human interleukin 18 by poxvirus interleukin 18-binding protein. *Proc Natl Acad Sci U S A.* 2008;105(52):20711-5.

81. Tobin G. FDA approves Gamifant® (emapalumab-lzsg) as first-ever treatment for adults and children with Macrophage Activation Syndrome in Still's disease. https://www.sobi.com/en/press-releases/fda-approves-gamifantr-emapalumab-lzsg-first-ever-

treatment-adults-and-children-macrophage-activation-syndrome-stills-disease-2342991. Accessed 6/29/25.

82. Sepulveda FE, Garrigue A, Maschalidi S, Garfa-Traore M, Menasche G, Fischer A, et al. Polygenic mutations in the cytotoxicity pathway increase susceptibility to develop HLH immunopathology in mice. *Blood.* 2016;127(17):2113-21.

83. Gasmi B, and Kleiner DE. Liver Histology: Diagnostic and Prognostic Features. *Clin Liver Dis.* 2020;24(1):61-74.

84. Bezman NA, Kim CC, Sun JC, Min-Oo G, Hendricks DW, Kamimura Y, et al. Molecular definition of the identity and activation of natural killer cells. *Nat Immunol.* 2012;13(10):1000-9.

Figure Legends:

Figure 1. NK cells are decreased and abnormal in resting *Il18*^{tg} mice.

(**A**) Absolute number of NK cells from various organs and peripheral blood mononuclear cells (PBMC, cells/mL). (**B**) Representative splenic NK cell expression of CD11b and IL-18Rα and aggregate proportion of IL-18Rα+ NK cells. (**C-D**) Representative and aggregate plots of NK maturity markers CD27 and CD11b on NK cells from bone marrow and spleen. Black arrow represents the progression of NK cell maturation. (**E**) Ratio of live *Il18*^{tg} NK cells to live WT NK cells (average of WT technical replicates, from the same experiment) after 5 hours in culture. Each dot represents a biological replicate. Significance: (A) Multiple lognormal t-tests (A) and multiple unpaired t-tests (B) of "WT vs. *Il18*^{tg}" within each organ. (C-D) 2-way ANOVA (inset box) with Šídák's pairwise post-test (line with p-value) of "WT vs *Il18*^{tg}" within each phenotype. (E) Mann Whitney U-test. A-D: Representative of 4 independent experiments. E: Combined data from two independent experiments. "ns" = adjusted p-value < 0.05.

Figure 2. Globally increased CD8 T-cell activation in resting *Il18*^{tg} mice.

(**A**) Total CD8 T-cell numbers from various organs and peripheral blood mononuclear cells (PBMC, cells/mL). Representative contour plots (**B**, from spleen) and (**C**) aggregate data of CD44 and PD-1 defined subsets as a proportion of all CD8 T cells from various organs. (**D**) Absolute number of highly-activated CD44+ PD1+ CD8 T cells (**D**). Significance: (A,D) Multiple lognormal t-tests and (C) 2-way ANOVA (not shown) with Šídák's pairwise post-tests (line with p-value) of genotype within each phenotype. The only comparison shown is highly activated ($CD44^{+}PD\text{-}1^{+}$) CD8 T cells. Representative of 3 independent experiments. "ns" = adjusted p-value < 0.05.

Figure 3. Impaired NK activation and CD8 T-cell hyperactivation characterize the early response to mousepox infection of *Il18*^{tg} mice.

Adult mice were infected with mousepox (ECTV) and assessed 5 days post-infection for (**A**) NK cell number and proportion compared to other cell types (see also **Supplemental Figure 4**); (**B**) CD49b upregulation and proportion of CD49b+; (**C**) Viral RNA (see also **Supplemental Figure 5**); (**D**) plasma IFNg; and (**E**) splenic CD8 T-cell PD-1 and CD44 expression as proportion of total CD8 T Cells (left) and absolute number (right). (**F-H**) Mice were injected i.p. on days -1 and 2 with anti-NK1.1 (NK depleted) or control antibodies, infected with ECTV, and assessed at day 5 for viral RNA; CD8 T-cell activation, and blood IFNg. For PBMC, absolute number = cells/mL. Significance: 2-way ANOVA (inset box) with Šídák's pairwise post-tests (line with p-value) of genotype (A,B, E) or NK depletion (F-H); multiple lognormal t-tests (C), and unpaired t-test (D). (E) For proportion of total CD8 T cells, only CD44+ PD-1+ CD8 T cells were assessed. (A,B,E). Homeostatic data in A & E are reproduced from Fig. 1A & Fig. 2C-D, respectively. A,B,E: Data representative of 2 independent experiments; and C,D,F-H: combined from 2 independent experiments. "ns" = adjusted p-value < 0.05.

Figure 4. *Il18*^{tg} mice ultimately develop fulminant HLH/MAS with impaired viral control following mousepox infection.

Adult mice were infected with mousepox (ECTV) and assessed for daily weight loss (**A**) and survival (**B**), (n=26 WT and 28 *Il18*^{tg}); hemoglobin (HB) and platelet count (PLT) (**C**), gross abdominal morphology (**D**), and liver necrosis score (**E**). L=lymphocytic infiltration and N=area of necrosis. Mice were also assessed longitudinally for liver NK cells (**F**), activated CD8 T Cells

(**G**), monocytes (**H**), liver and spleen ECTV RNA (**I**), and serum IFNg (**J**); n=2-5 mice/day. Dotted line in (J) represents threshold of detection. Significance: (A, F-J) Mixed Effects Model including genotype, time, and outcome variable. P-value represents only independent effect of genotype, (B) Kaplan-Meier test, (C) unpaired t-tests, and (E) Mann Whitney U-test. Homeostatic and Day 5 data in F, G, I, and J are supplemented by data reproduced from Figures 1A, 2D, and 3A,C,D. A-E, I-J: Data combined from 4 independent experiments; F-H: representative of 4 independent experiments.

Figure 5. *Il18bp*^{KO} mice, despite normal basal NK and CTL, develop severe HLH/MAS with impaired viral control following mousepox infection.

Homeostatic NK cell numbers from various organs (**A**). Adult mice were infected with mousepox (ECTV) and assessed 5 days later for (**B**) splenic NK cell number, CD49b expression, and CD49b+ proportion; and (**C**) splenic viral load. Weights were assessed longitudinally (**D**). On day 8, we assessed hemoglobin (HB) and platelet count (PLT) (**E**), serum IFNg (**F**), liver injury (**G**), splenic CD8 T-cell PD-1 and CD44 expression as proportion of total CD8 T cells (left) and absolute number (right) (**H**), and splenic ECTV RNA (**I**). Dotted line in (F) represents threshold of detection. L= lymphocytic infiltration and N=necrosis. Significance: Multiple lognormal t-tests (A); unpaired t-test (B,E); lognormal t-test (C,I); Mixed Effects Model including genotype, time, and outcome variable where P-value represents only independent effect of genotype (D); 2-way ANOVA (inset box) with Šídák's pairwise post-tests comparing genotype (line with p-value) (F,H); or Mann-Whitney U-test (G). Only $CD44^{+}PD1^{+}$ CD8 T Cells were compared in 2-way ANOVA shown on the left (H). All data representative of 2 independent experiments. “ns” = adjusted p-value < 0.05.

Figure 6. Failed mousepox-specific CD8 T-cell expansion and function in mice with excess IL-18.

Il18^{tg} mice were infected with mousepox (ECTV) and evaluated periodically (**A**) and *Il18bp*^{KO} mice on Day8 (**D**) for B8R peptide-specific CD8 T cells. (**B,C,E**) On day 7-8, mice underwent in vivo killing assay (**see Methods**). Dots represent (recovered control splenocytes) / (recovered ECTV-peptide loaded splenocytes) from the same animal. (**F**) Correlation between weight loss and B8R-tetramer^{+} CD8 T cells recovered in spleens on day 8 amongst *Il18bp*^{KO} mice. Significance: Mixed Effects Model including genotype, time, and outcome variable where p-value represents only independent effect of genotype (A), unpaired t-test (B, D-E), and multiple unpaired t test (C) and linear regression (F). A & C-F: data representative of 3 & 2 independent experiments, respectively; and B: data combined from 2 independent experiments. "ns" = adjusted p-value < 0.05.

Figure 7. Early and persistent CTL hyperactivation belie failed mousepox-specific CD8 T-cell responses in *Il18*^{tg} mice.

WT and *Il18*^{tg} mice were infected with mousepox (ECTV) and livers and spleens from two mice/genotype/timepoint were evaluated by flow cytometry. Data from 10,000 randomly-selected live cells per organ per mouse (10,000 cells x 2 organs/mouse x 4mice/day x 6 days = 480,000 total cells) were concatenated. From this, we gated CD8 T cells and entered these into an annotated Uniform Manifold Approximation and Projection (UMAP) (**A**). Normalized fluorescence intensity of the indicated surface targets (**B**). Progression of CD8 T-cell abundance

and location within the UMAP over time and by genotype (**C**). Dotted outlines indicate the location of B8R peptide-specific CD8 T cells.

Figure 8. Transfer of ex vivo-expanded NK cells partially rescues *Il18*^{tg} mice from mousepox-triggered immunodeficiency and mortality.

(**A**) Experimental design: WT NK cells were expanded ex vivo over 7-10 days and adoptively transferred into *Il18*^{tg} mice one day prior to mousepox (ECTV) infection. Mice were assessed for survival (**B**) and weight loss (**C**); (n=7 WT, 7 *Il18*^{tg} and 6 *Il18*^{tg} + NK cells). 3-4 days post infection, transferred NK cells were recovered in livers but not spleens (**D** & data not shown). (**E**) Representative flow plots compare pre-transfer and recovered NK cells for IL-18Rα, CD49b, and CD11b expression. On Day 8, we evaluated B8R-specific CD8 T cells (**F**), ECTV RNA (**G**), and serum IFNg (**H**). Dotted lines represent median values of WT mice from the same experiment and time point. Significance: All comparisons between "*Il18*^{tg}" and "*Il18*^{tg} + WT NK cells": (B) Kaplan-Meier test, (C) mixed effects model including genotype, time, and outcome variable where p-value represents only independent effect of genotype; (F, H) unpaired t-test; (G) lognormal t-test. B,D,F-H & C: data compiled from 2 and 4 independent experiments, respectively. "ns" = adjusted p-value < 0.05.

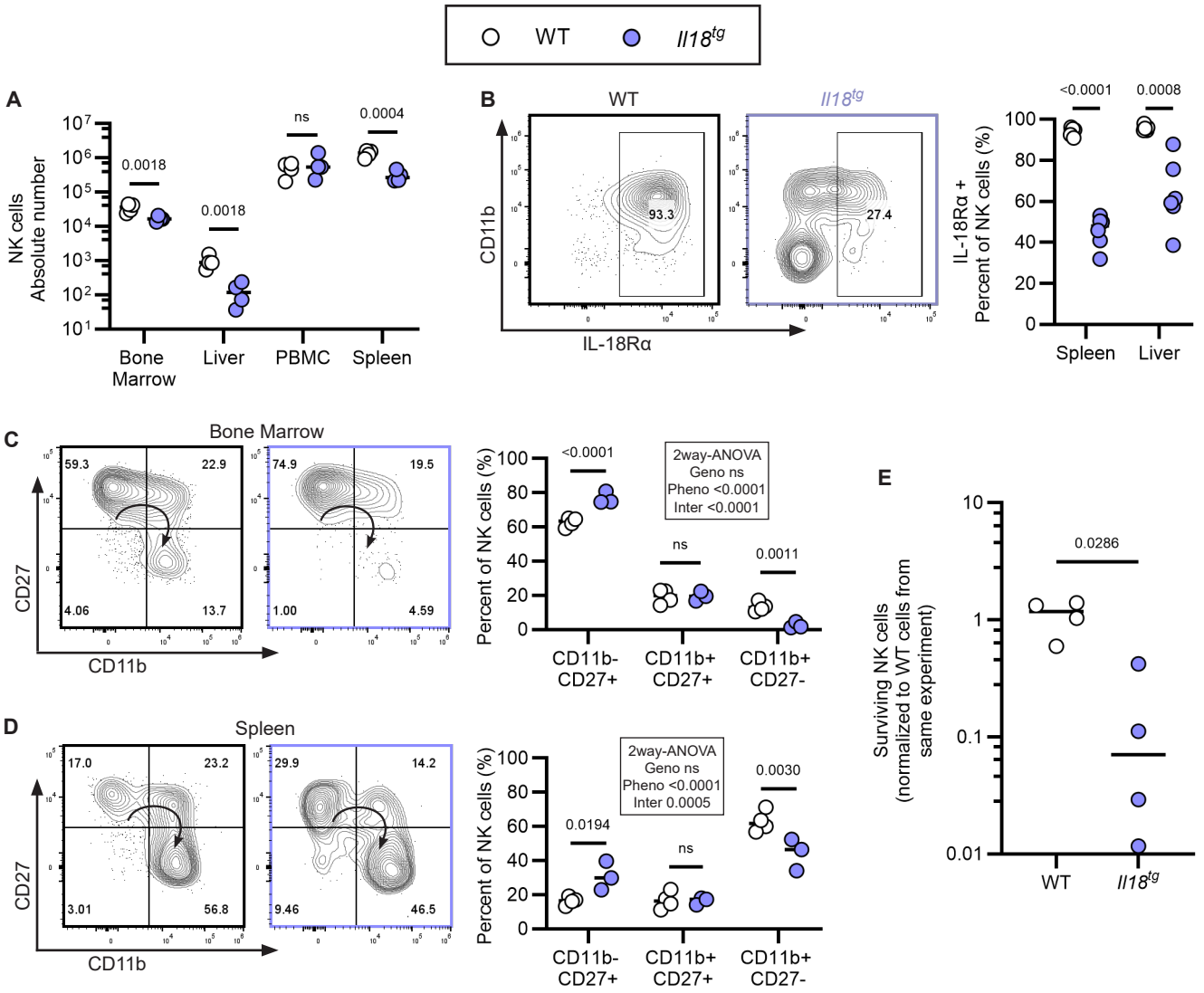


Figure 1. NK cells are decreased and abnormal in resting *Il18*^{tg} mice. (**A**) Absolute number of NK cells from various organs and peripheral blood mononuclear cells (PBMC, cells/mL). (**B**) Representative splenic NK cell expression of CD11b and IL-18Rα and aggregate proportion of IL-18Rα+ NK cells. (**C-D**) Representative and aggregate plots of NK maturity markers CD27 and CD11b on NK cells from bone marrow and spleen. Black arrow represents the progression of NK cell maturation. (**E**) Ratio of live *Il18*^{tg} NK cells to live WT NK cells (average of WT technical replicates, from the same experiment) after 5 hours in culture. Each dot represents a biological replicate. Significance: (A) Multiple lognormal t-tests (A) and multiple unpaired t-tests (B) of "WT vs. *Il18*^{tg}" within each organ. (C-D) 2-way ANOVA (inset box) with Šídák's pairwise post-test (line with p-value) of "WT vs *Il18*^{tg}" within each phenotype. (E) Mann Whitney U-test. A-D: Representative of 4 independent experiments. E: Combined data from two independent experiments. "ns" = adjusted p-value < 0.05.

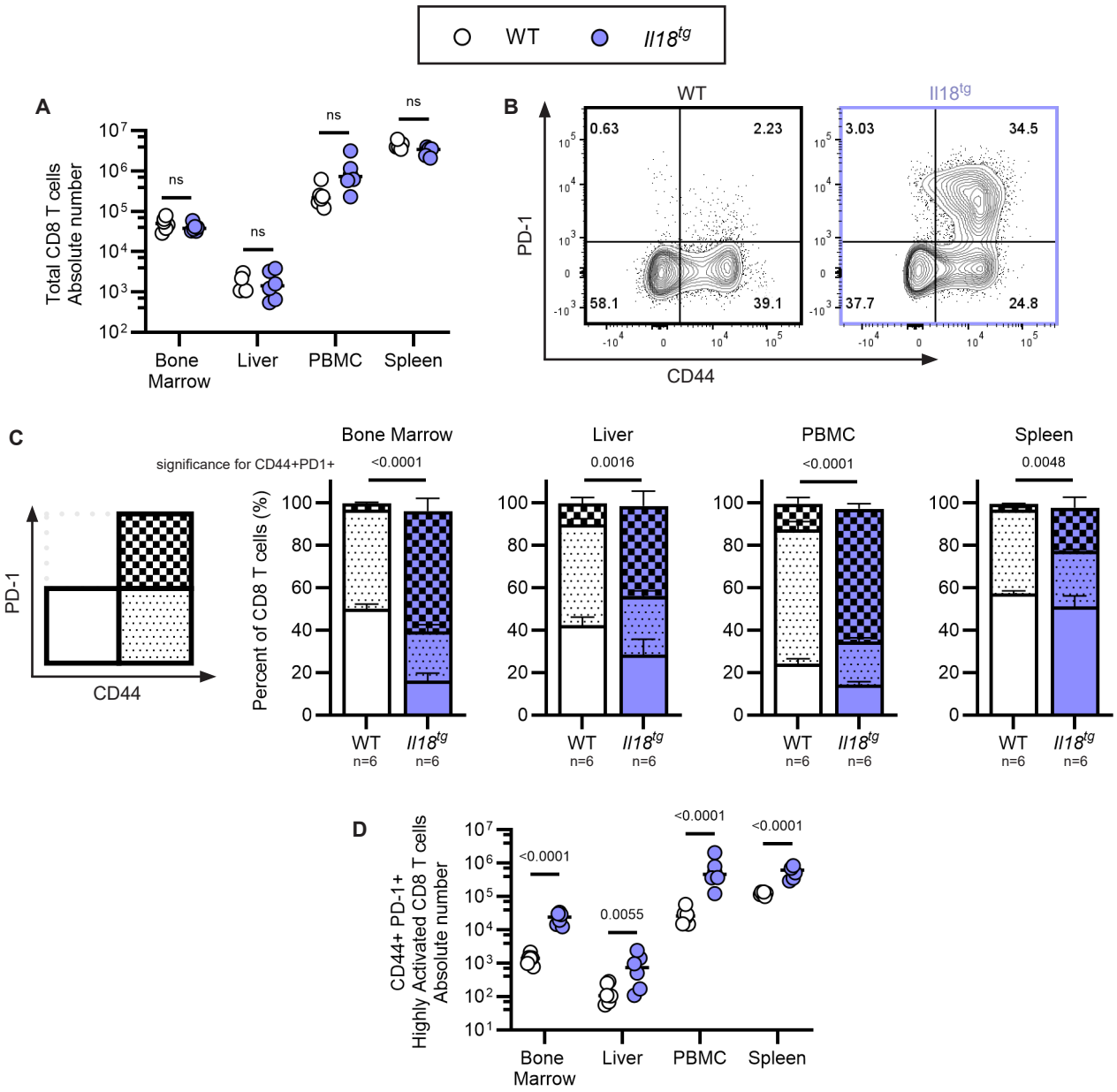


Figure 2. Globally increased CD8 T-cell activation in resting *Il18*^{tg} mice. (**A**) Total CD8 T-cell numbers from various organs and peripheral blood mononuclear cells (PBMC, cells/mL). Representative contour plots (**B**, from spleen) and (**C**) aggregate data of CD44 and PD-1 defined subsets as a proportion of all CD8 T cells from various organs. (**D**) Absolute number of highly-activated CD44+ PD1+ CD8 T cells (**D**). Significance: (A,D) Multiple lognormal t-tests and (C) 2-way ANOVA (not shown) with Šídák's pairwise post-tests (line with p-value) of genotype within each phenotype. The only comparison shown is highly activated (CD44^{+}PD-1^{+}) CD8 T cells. Representative of 3 independent experiments. "ns" = adjusted p-value < 0.05.

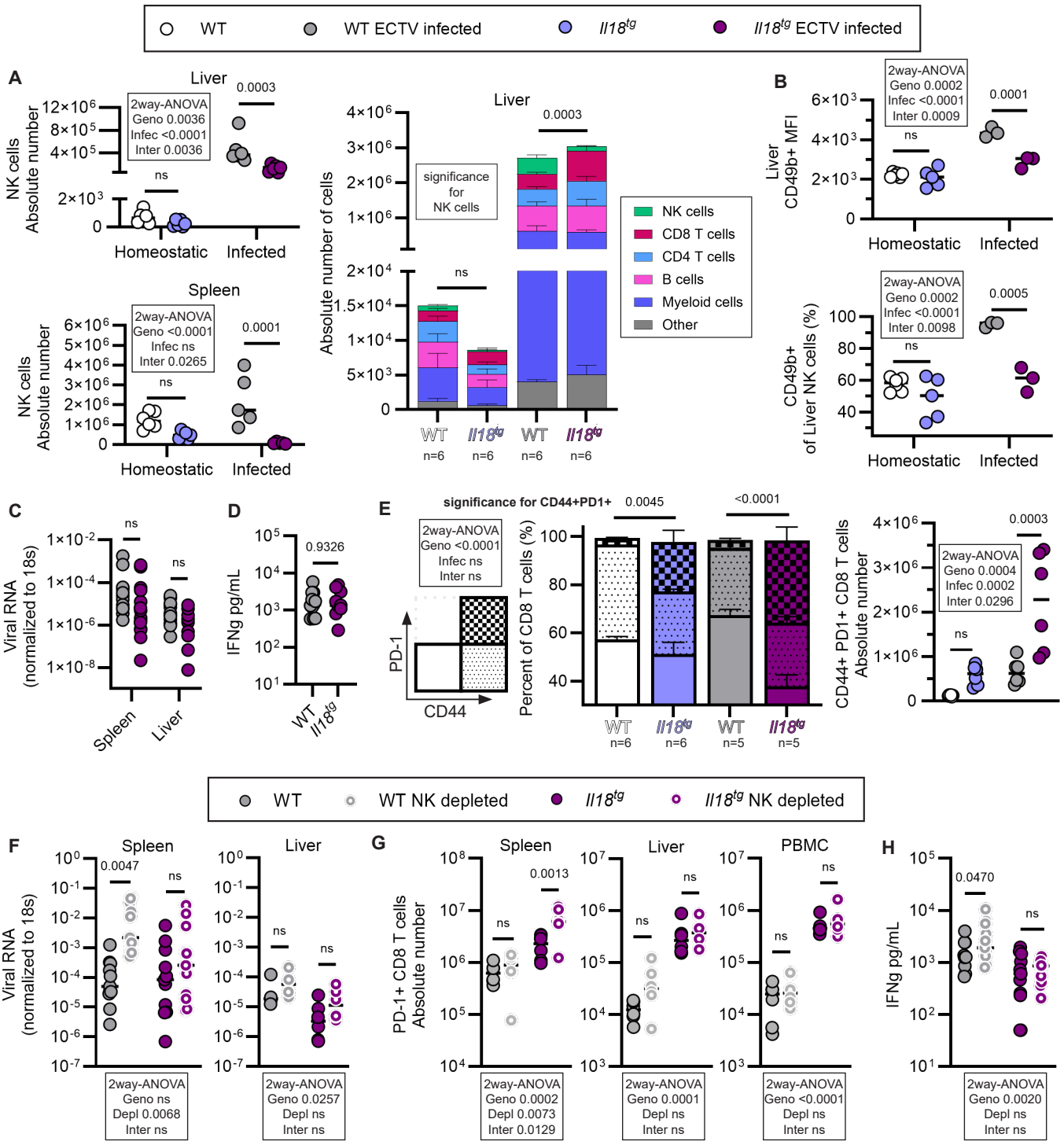


Figure 3. Impaired NK activation and CD8 T-cell hyperactivation characterize the early response to mousepox infection of *Il18*^{tg} mice. Adult mice were infected with mousepox (ECTV) and assessed 5 days post-infection for (**A**) NK cell number and proportion compared to other cell types (see also **Supplemental Figure 4**); (**B**) CD49b upregulation and proportion of CD49b+; (**C**) Viral RNA (see also **Supplemental Figure 5**); (**D**) plasma IFNg; and (**E**) splenic CD8 T-cell PD-1 and CD44 expression as proportion of total CD8 T Cells (left) and absolute number (right). (**F-H**) Mice were injected i.p. on days -1 and 2 with anti-NK1.1 (NK depleted) or control antibodies, infected with ECTV, and assessed at day 5 for viral RNA; CD8 T-cell activation, and blood IFNg. For PBMC, absolute number = cells/mL. Significance: 2-way ANOVA (inset box) with Šídák's pairwise post-tests (line with p-value) of genotype (A,B, E) or NK depletion (F-H); multiple lognormal t-tests (C), and unpaired t-test (D). (E) For proportion of total CD8 T cells, only CD44+ PD-1+ CD8 T cells were assessed. (A,B,E). Homeostatic data in A & E are reproduced from Fig. 1A & Fig. 2C-D, respectively. A,B,E: Data representative of 2 independent experiments; and C,D,F-H: combined from 2 independent experiments. "ns" = adjusted p-value < 0.05.

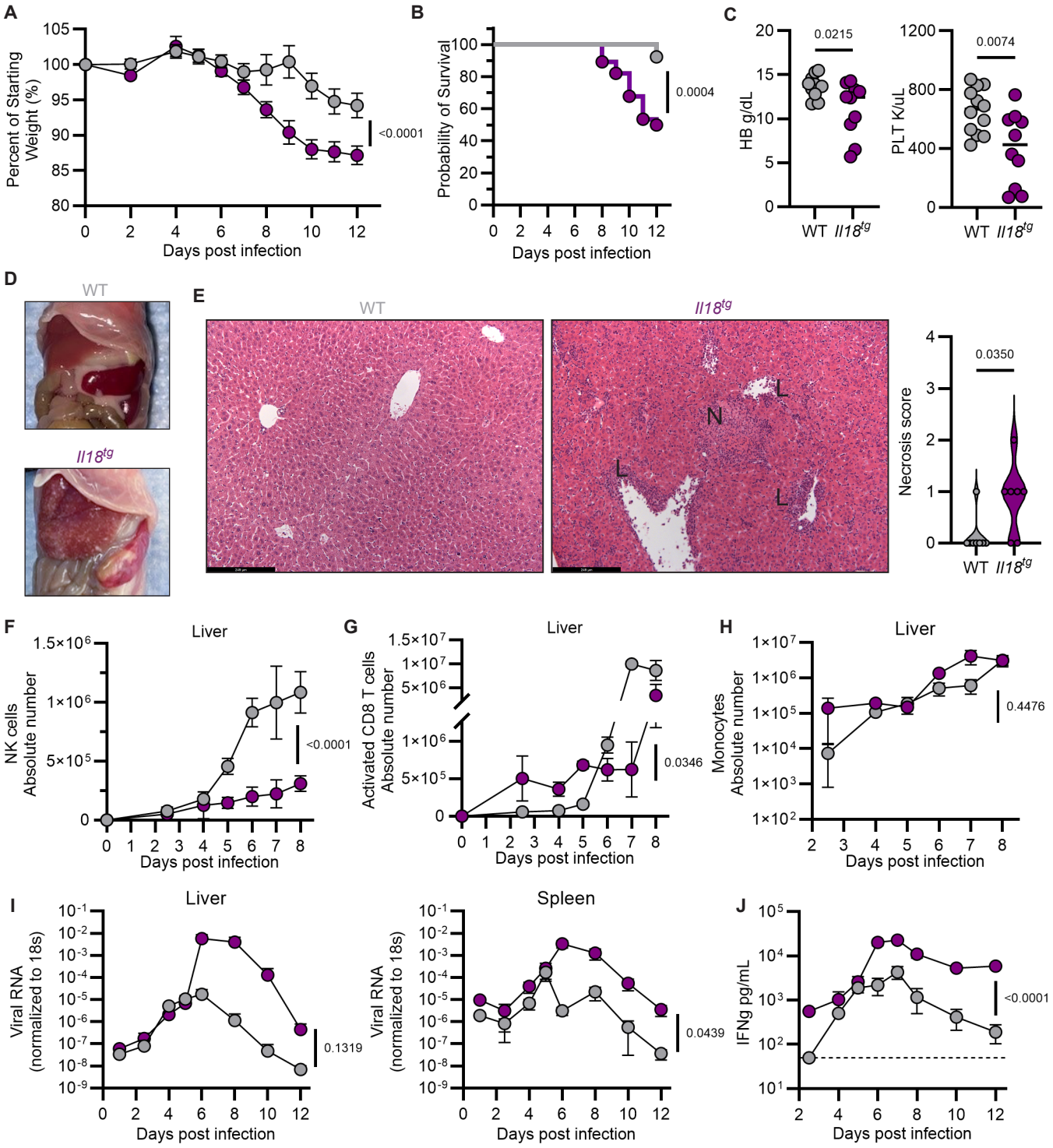


Figure 4. *Il18*^{tg} mice ultimately develop fulminant HLH/MAS with impaired viral control following mousepox infection. Adult mice were infected with mousepox (ECTV) and assessed for daily weight loss (**A**) and survival (**B**), (n=26 WT and 28 *Il18*^{tg}); hemoglobin (HB) and platelet count (PLT) (**C**), gross abdominal morphology (**D**), and liver necrosis score (**E**). L=lymphocytic infiltration and N=area of necrosis. Mice were also assessed longitudinally for liver NK cells (**F**), activated CD8 T Cells (**G**), monocytes (**H**), liver and spleen ECTV RNA (**I**), and serum IFNg (**J**); n=2-5 mice/day. Dotted line in (J) represents threshold of detection. Significance: (A, F-J) Mixed Effects Model including genotype, time, and outcome variable. P-value represents only independent effect of genotype, (B) Kaplan-Meier test, (C) unpaired t-tests, and (E) Mann Whitney U-test. Homeostatic and Day 5 data in F, G, I, and J are supplemented by data reproduced from Figures 1A, 2D, and 3A,C,D. A-E, I-J: Data combined from 4 independent experiments; F-H: representative of 4 independent experiments.

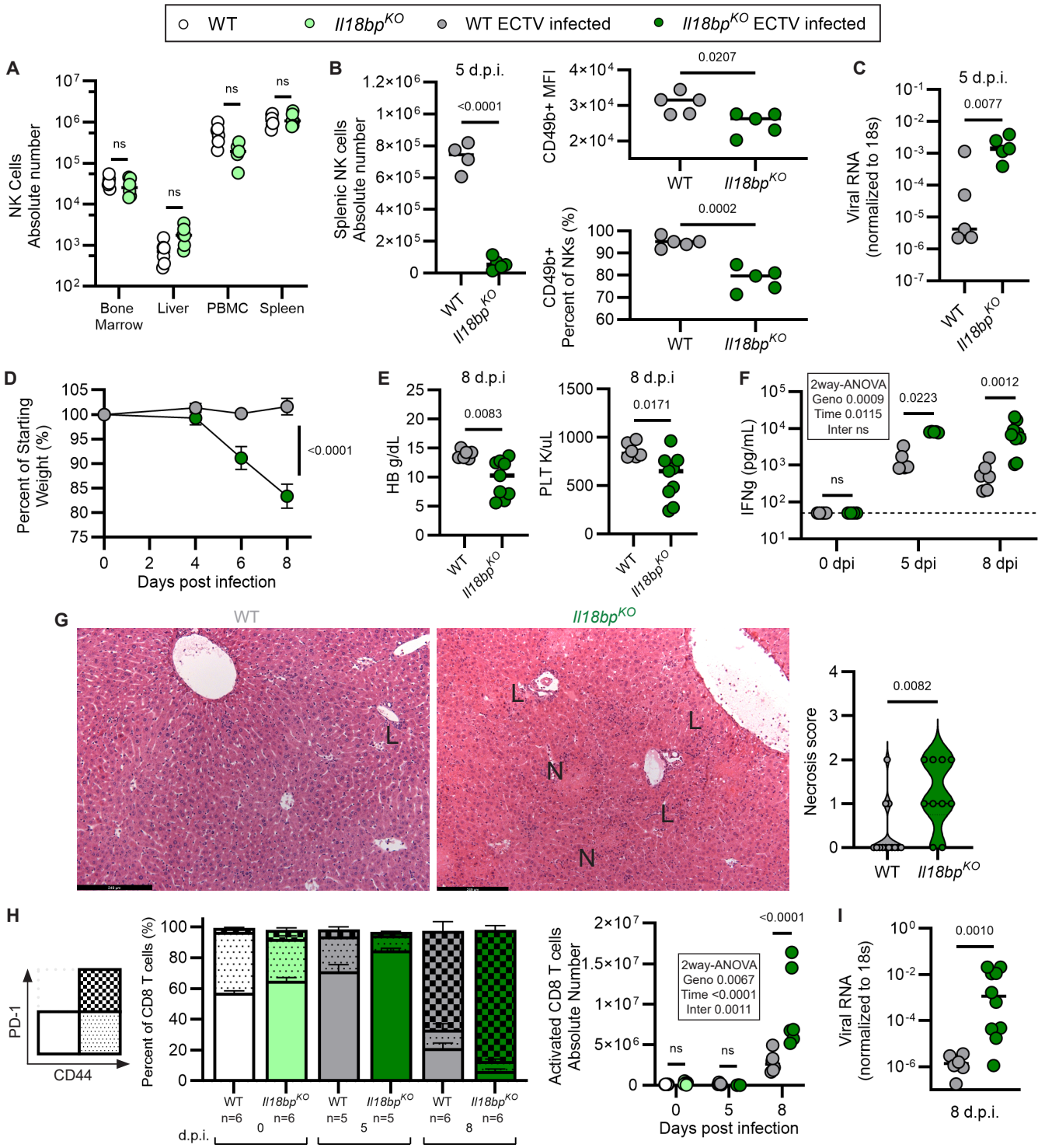


Figure 5. *Il18bp*^{KO} mice, despite normal basal NK and CTL, develop severe HLH/MAS with impaired viral control following mousepox infection. Homeostatic NK cell numbers from various organs (**A**). Adult mice were infected with mousepox (ECTV) and assessed 5 days later for (**B**) splenic NK cell number, CD49b expression, and CD49b+ proportion; and (**C**) splenic viral load. Weights were assessed longitudinally (**D**). On day 8, we assessed hemoglobin (HB) and platelet count (PLT) (**E**), serum IFNg (**F**), liver injury (**G**), splenic CD8 T-cell PD-1 and CD44 expression as proportion of total CD8 T cells (left) and absolute number (right) (**H**), and splenic ECTV RNA (**I**). Dotted line in (F) represents threshold of detection. L= lymphocytic infiltration and N=necrosis. Significance: Multiple lognormal t-tests (A); unpaired t-test (B,E); lognormal t-test (C,I); Mixed Effects Model including genotype, time, and outcome variable where P-value represents only independent effect of genotype (D); 2-way ANOVA (inset box) with Šídák's pairwise post-tests comparing genotype (line with p-value) (F,H); or Mann-Whitney U-test (G). Only CD44^{+}PD1^{+} CD8 T Cells were compared in 2-way ANOVA shown on the left (H). All data representative of 2 independent experiments. "ns" = adjusted p-value < 0.05.

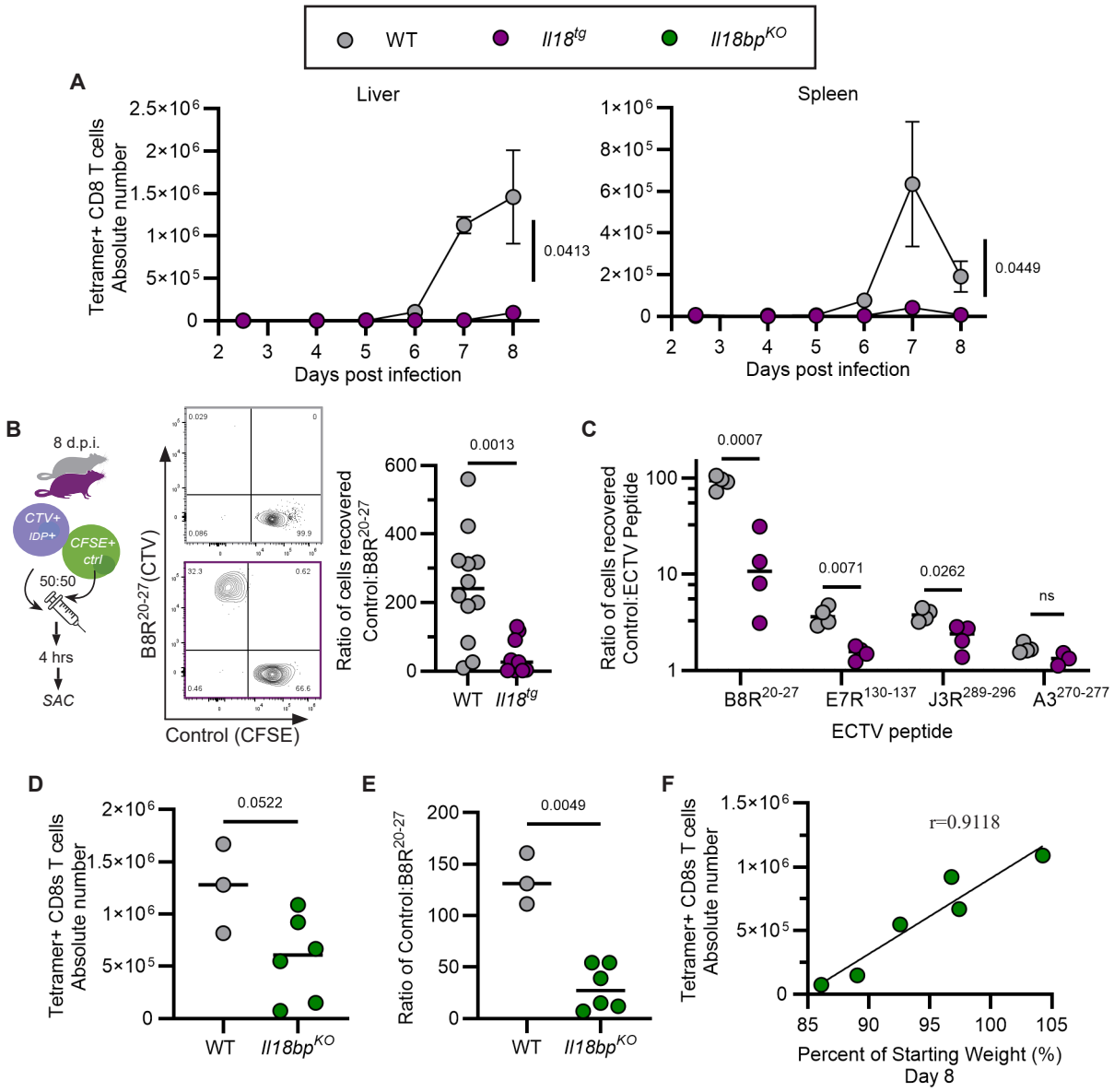


Figure 6. Failed mousepox-specific CD8 T-cell expansion and function in mice with excess IL-18. *Il18*^{tg} mice were infected with mousepox (ECTV) and evaluated periodically (**A**) and *Il18bp*^{KO} mice on Day8 (**D**) for B8R peptide-specific CD8 T cells. (**B,C,E**) On day 7-8, mice underwent in vivo killing assay (**see Methods**). Dots represent (recovered control splenocytes) / (recovered ECTV-peptide loaded splenocytes) from the same animal. (**F**) Correlation between weight loss and B8R-tetramer^{+} CD8 T cells recovered in spleens on day 8 amongst *Il18bp*^{KO} mice. Significance: Mixed Effects Model including genotype, time, and outcome variable where p-value represents only independent effect of genotype (A), unpaired t-test (B, D-E), and multiple unpaired t test (C) and linear regression (F). A & C-F: data representative of 3 & 2 independent experiments, respectively; and B: data combined from 2 independent experiments. "ns" = adjusted p-value < 0.05.

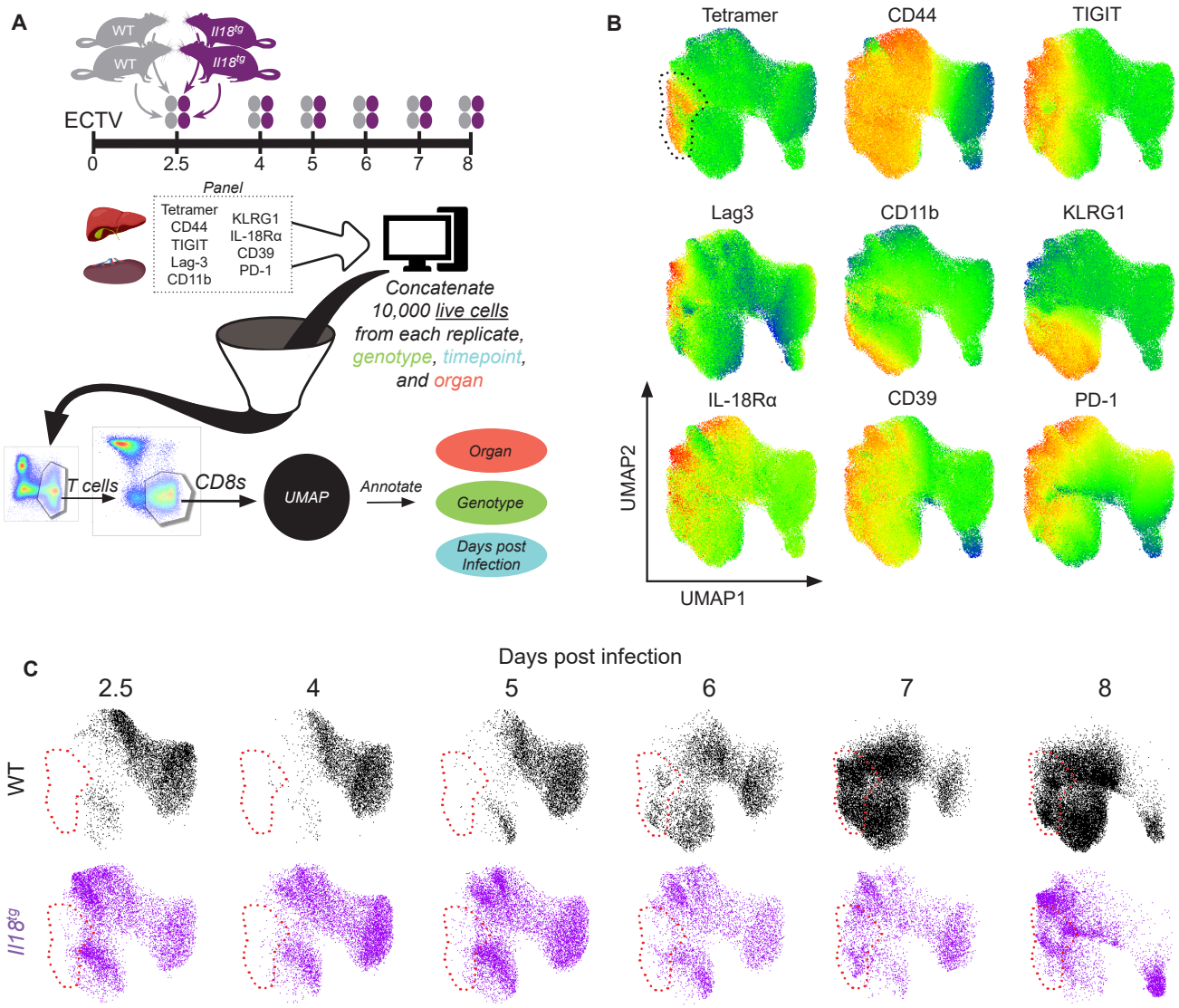


Figure 7. Early and persistent CTL hyperactivation belie failed mousepox-specific CD8 T-cell responses in *Il18*^{tg} mice. WT and *Il18*^{tg} mice were infected with mousepox (ECTV) and livers and spleens from two mice/genotype/timepoint were evaluated by flow cytometry. Data from 10,000 randomly-selected live cells per organ per mouse (10,000 cells x 2 organs/ mouse x 4mice/day x 6 days = 480,000 total cells) were concatenated. From this, we gated CD8 T cells and entered these into an annotated Uniform Manifold Approximation and Projection (UMAP) (**A**). Normalized fluorescence intensity of the indicated surface targets (**B**). Progression of CD8 T-cell abundance and location within the UMAP over time and by genotype (**C**). Dotted outlines indicate the location of B8R peptide-specific CD8 T cells.

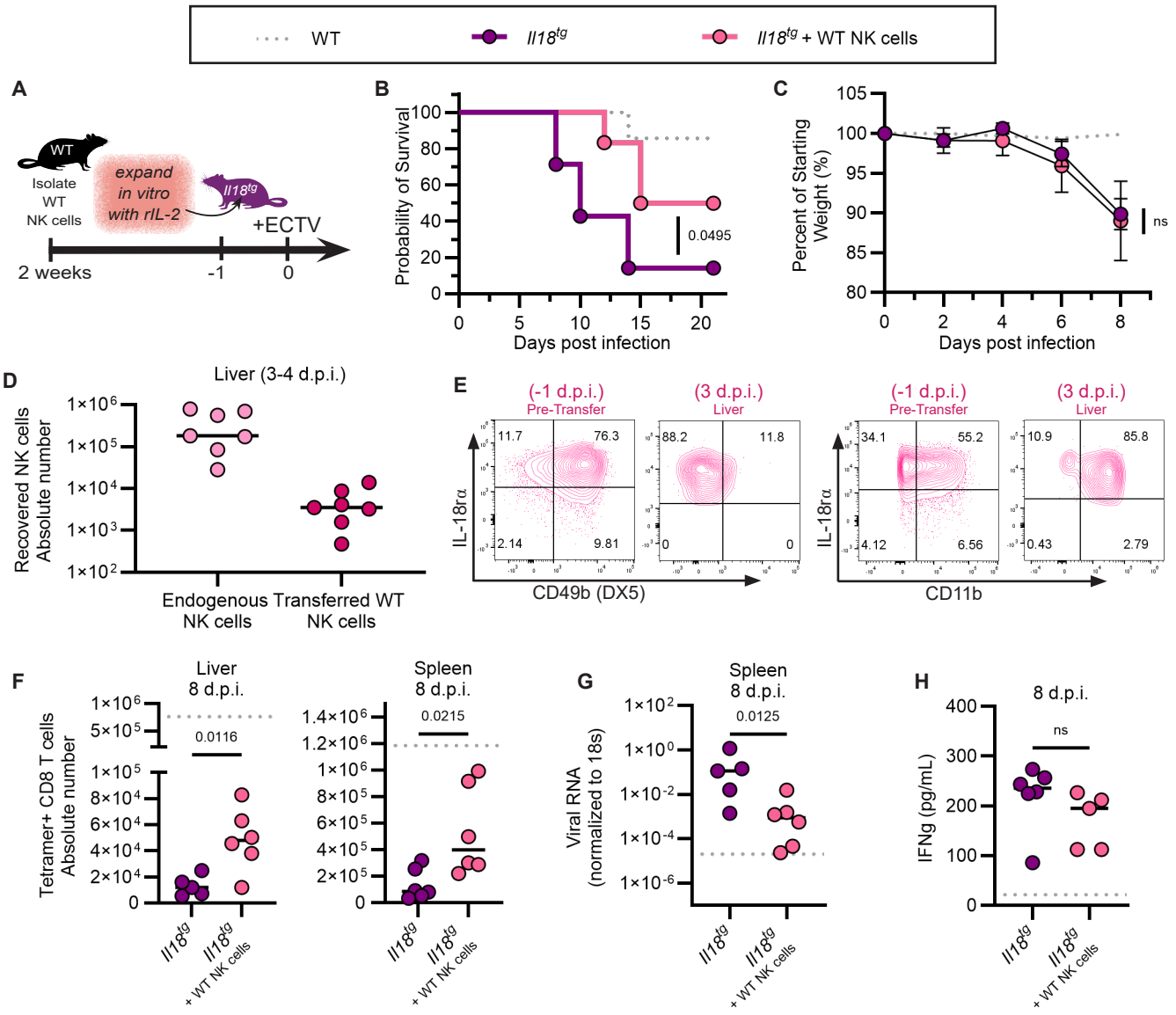


Figure 8. Transfer of ex vivo-expanded NK cells partially rescues *Il18*^{tg} mice from mousepox-triggered immunodeficiency and mortality. (**A**) Experimental design: WT NK cells were expanded ex vivo over 7-10 days and adoptively transferred into *Il18*^{tg} mice one day prior to mousepox (ECTV) infection. Mice were assessed for survival (**B**) and weight loss (**C**); (n=7 WT, 7 *Il18*^{tg} and 6 *Il18*^{tg} + NK cells). 3-4 days post infection, transferred NK cells were recovered in livers but not spleens (**D** & data not shown). (**E**) Representative flow plots compare pre-transfer and recovered NK cells for IL-18Rα, CD49b, and CD11b expression. On Day 8, we evaluated B8R-specific CD8 T cells (**F**), ECTV RNA (**G**), and serum IFNg (**H**). Dotted lines represent median values of WT mice from the same experiment and time point. Significance: All comparisons between "*Il18*^{tg}" and "*Il18*^{tg} + WT NK cells": (B) Kaplan-Meier test, (C) mixed effects model including genotype, time, and outcome variable where p-value represents only independent effect of genotype; (F, H) unpaired t-test; (G) lognormal t-test. B,D,F-H & C: data compiled from 2 and 4 independent experiments, respectively. "ns" = adjusted p-value < 0.05.